DOI:10.1130/G45329.1

Perovskite U-Pb and Sr-Nd isotopic perspectives on melilitite magmatism and outward growth of the Tibetan plateau

Dong Liu[1,*], Zhidan Zhao[1,*], Yaoling Niu[1, 2], Di-Cheng Zhu[1], and Xian-Hua Li[3]

[1]State Key Laboratory of Geological Processes and Mineral Resources, and School of Earth Science and Resources, China University of Geosciences, Beijing 100083, China

[2]Department of Earth Sciences, Durham University, Durham DH1 3LE, UK

[3]State Key Laboratory of Lithospheric Evolution, Institute of Geology and Geophysics, Chinese Academy of Sciences, Beijing 100029, China

*E-mail: d.liu@cugb.edu.cn; zdzhao@cugb.edu.cn

ABSTRACT

Mantle-derived alkaline magmatism along major strike-slip faults carries important messages on the lateral growth of the Tibetan plateau. Here we use the geochemistry of perovskites from West Qinling melilitite to probe into the nature and dynamics of sub-lithospheric mantle beneath the northeastern Tibetan plateau. The texture and chemical composition of perovskites indicate their early crystallization from a CO_2-rich melilitite magma. Most perovskite crystals have moderately depleted Sr-Nd isotopic compositions whereas a few grains exhibit high $^{87}Sr/^{86}Sr_i$ and low $\varepsilon_{Nd}(t)$. Together with the bulk-rock geochemistry of the melilitite, the perovskite Sr-Nd isotope data can be used to show that the primary magma parental to the melilitite must have derived from seafloor subduction-modified asthenosphere and underwent interaction with lithospheric mantle during ascent. In situ U-Pb dating of the perovskites demonstrates the temporal correlation between the melilitite magmatism and the Kunlun strike-slip faulting in the early-Miocene. These findings indicate the fundamental importance of continued Indian-Asia convergence in causing outward growth of the Tibetan plateau through strike-slip fault displacement and in reactivating the long-lived lithospheric zones of weakness for draining low-volume asthenosphere-derived melts.

INTRODUCTION

The outward growth and strike-slip extrusion of the Tibetan plateau are accompanied by formation of low-volume and deeply-rooted alkaline magmatism (e.g., Wang et al., 2001; Mahéo et al., 2009; Dai et al., 2017). These alkaline rocks can offer valuable insights into the mantle dynamics (Molnar et al., 1993; Tapponnier et al., 2001) and allow a better understanding of the tectonic and topographic evolution of the India-Asia collision zone (see Wang et al., 2013, for a review). However, the inevitable contamination and hydrothermal alteration at crustal levels make it difficult to constrain the nature of sources through bulk-rock data of mantle-derived rocks (Tappe et al., 2012; Sun et al., 2014). The lack of accurate and precise age data on alkaline rocks with mantle affinity also leads to ambiguities in their correlations with tectonic processes on various scales, preventing us from understanding the way in which the Tibetan plateau may have grown laterally in space and time.

Perovskite ($CaTiO_3$) is a common accessory mineral in SiO_2-undersaturated rocks and serves as a major carrier of Th, U, Sr, and rare earth elements (Chakhmouradian et al., 2013). It is thus suitable for U-Th-Pb dating and its radiogenic isotopes can also provide reliable information about magmatic sources and processes (Yang et al., 2009; Tappe et al., 2012, 2018). Here we present a combined study of in situ U-Pb dating, trace element analysis, and Sr-Nd isotope compositions on perovskites extracted from the melilitite in the West Qinling orogenic belt. These data, together with seismic tomography across the Kunlun fault zone, provide insights into the geochemical and dynamic evolution of the upper mantle beneath the northeastern Tibetan Plateau. This study also presents the first perovskite U-Pb ages for melilitite magmatism on the greater Tibetan Plateau, highlights the critical role of trans-lithospheric lineaments in the generation and emplacement of postcollisional alkaline magmatism, and gives a detailed pattern for the outward growth of the plateau in space and time.

TECTONIC SETTING AND SAMPLE DESCRIPTIONS

The Qinling orogenic belt stretches eastward through the Dabie orogen, connects with the Kunlun orogen to the west, and preserves numerous metamorphic and magmatic records of Proterozoic-Mesozoic seafloor subduction and continental collision episodes (Dong and Santosh 2016). The western part of the Qinling orogenic belt is a conjunction region of the Tibetan plateau, the North and South China blocks (Fig. 1A). Since the Cenozoic, the northeastern Tibetan plateau has undergone significant lithospheric deformation and tectonic rotation, and has developed numerous thrust and strike-slip faults to accommodate the continued India-Asia convergence (Tapponnier et al., 2001; Wang et al., 2013). The Kunlun fault (> 1500 km long) is a prominent left-lateral strike-slip fault zone on the northern and northeastern Tibetan Plateau. It propagates along the plate boundary between the Songpan Ganzi-Hohxil terrane and eastern Kunlun, and extends eastward into the West Qinling orogenic belt (Fig. 1A). A thermochronological study on the exhumation history associated with the Kunlun strike-slip faulting indicates that this sinistral fault may have initiated in the early-Miocene or earlier (20–15 Ma) with a total offset of 100–300 km at a high Quaternary slip rate (≥ 10 mm/yr) (Duvall et al., 2013).

Postcollisional potassic and ultrapotassic volcanic centers are scattered along the west segment of the Kunlun fault in the Songpan Ganzi-Hohxil terrane (Fig. 1A), giving varying K-Ar and Ar-Ar ages ranging from 24.6 Ma to 0.30 Ma (Table DR1). To the east, several rhomb-shaped Cenozoic basins have developed along and adjacent to the Kunlun fault. The West Qinling melilitite, which commonly occurs as volcanic pipes and lava flows, are distributed in the Tianshui-Lixian basin (Fig. DR1). Mantle xenoliths and carbonate ocelli can be identified from melilititic lava, and, in some area, it is found to be interbedded with extrusive Ca-carbonatites (Fig. DR2). Melilitite samples have a porphyritic texture with phenocrysts dominated by pyroxenes, olivine, and minor phlogopite in a fine-grained groundmass. Their groundmass mineralogy includes melilite, nepheline, leucite, perovskite, and Fe-Ti oxides. The melilitite and shoshonite in West Qinling yield K-Ar and Ar-Ar eruption ages of 23.2–8.7 Ma (Table DR1 and references therein).

METHODS AND RESULTS

Bulk-rock major and trace element compositions of melilitite samples were measured at China University of Geosciences in Wuhan. Perovskites extracted from the melilitite were mounted in epoxy resin and selected for in situ analysis at the Institute of Geology and Geophysics, Chinese Academy of Sciences. Analytical methods and results were given in the Data Repository.

The West Qinling melilitite is a suite of SiO_2-undersaturated volcanic rocks with low Al_2O_3 (as low as 7.65 wt.%), high MgO (12.7–18.5 wt.%), and high CaO contents (up to 14.2 wt.%) (Table DR2). They have lower K_2O/Na_2O (0.5–1) and plot in the compositional fields of melilitite and nephelinite (Fig. DR3). The primitive mantle normalized trace element patterns of the melilitite are characterized by relative enrichment of large ion lithophile elements (LILEs) and light rare earth elements (LREEs), with weak negative anomalies in Rb, Zr, Hf, and Ti (Fig. DR3).

Melilititic perovskites commonly grow as euhedral and subhedral grains of varying size (50–200 μm). They are homogeneous and do not show oscillatory zoning in

DOI:10.1130/G45329.1

back-scattered electron (BSE) images (Fig. DR4). Mineral inclusions are rare, and alterations are not observed in these unzoned grains. The analyzed grains are almost pure $CaTiO_3$ (91.3–97.6 mol%) with minor SiO_2 (<0.17 wt.%) and Na_2O (0.21–1.35 wt.%) (Table DR3). All grains exhibit negative Rb, Ba, Pb, Sr, Zr, Hf, and Y anomalies, showing elevated LREEs relative to heavy (H)REEs (Fig. 2).

Perovskites have varying Th (10.3–1462 ppm) and U (50.8–333 ppm) contents and a wide range of Th/U (0.09–23.6, Tables DR3 and DR4). The isotopic data for each sample define an array that intercepts the inverse concordia curve in the Tera-Wasserburg diagram and yields lower intercept ages of 15.93 ± 0.44 Ma to 20.06 ± 0.84 Ma (Fig. DR5). The weighted mean $^{206}Pb/^{238}U$ ages based on the ^{207}Pb-correction method vary from 16.19 ± 0.42 Ma to 20.35 ± 0.89 Ma, which agree well with lower intercept ages for each sample.

Unradiogenic Sr and radiogenic Nd isotopic compositions are obvious for the melilititic perovskites (Fig. 3). Except for a few grains (e.g., LX1506@12), the initial Sr isotopic ratios in perovskites ($^{87}Sr/^{86}Sr_i$ = 0.7026–0.7042, Table DR5) are lower than the bulk-rock values of the host melilitite ($^{87}Sr/^{86}Sr_i$ = 0.7037–0.7094) and mantle xenoliths ($^{87}Sr/^{86}Sr_i$ = 0.7040–0.7056). Both perovskites ($\varepsilon_{Nd}(t)$ = +0.1 to +7.5, Table DR6) and mantle xenoliths ($\varepsilon_{Nd}(t)$ = +1.3 to +7.1) have a narrower range in initial Nd isotopic variations than the melilitite ($\varepsilon_{Nd}(t)$ = –4.6 to +6.1).

DISCUSSION

DOI:10.1130/G45329.1

Textural and Trace Element Constraints on the Origin of Perovskite

Perovskite is an early crystallizing phase in SiO_2-undersaturated rocks, and its textural appearance and chemical composition may reflect the nature of primary magmas and rock-forming processes (Yang et al., 2009; Chakhmouradian et al., 2013). Texturally, the groundmass perovskites from the West Qinling melilitite are euhedral to subhedral and show uniform and smooth appearance in BSE images (Fig. DR4), which are in contrast with altered grains with spongy appearance (Yang et al., 2009). The lack of compositional zoning and inclusions of late crystallizing mineral (e.g., calcite and mica) also indicate that these unaltered perovskites were formed in the early stage of crystallization.

Geochemical compositions of the melilititic perovskites may provide further evidence for their primary magmatic origin (Fig. 2). The studied perovskites commonly have low SiO_2 and high CaO contents (Table DR3), which differ from those grains altered by post-crystallization hydrothermal events and preclude the occurrence of secondary alteration/modification (Yang et al., 2009). Moreover, the perovskites from the West Qinling melilitite show compositional similarity to those from kimberlites worldwide (Fig. 2). Experimental studies have showed that trace element systematics of perovskite is mainly controlled by melt composition and substitution mechanisms rather than pressure and temperature (Beyer et al., 2013; Chakhmouradian et al., 2013). We thus modeled their trace element compositions using bulk-rock data of melilitite samples and partition coefficients ($D_{element}$) with katungite (i.e., potassic olivine melilitite, Chakhmouradian et al., 2013). The modeling indicates that the distinctive signatures of the studied perovskites, including the enrichment of LREEs and relative deletions in Rb, Ba, Pb, Sr, Zr, and Hf, can be well reproduced by equilibrium crystallization from a melilitite parental magma (Fig. 2).

We also note that the melilititic perovskites display variably lower Th/U and higher HREEs concentrations than the modeled trace element pattern (Fig. 2). Growth in a primary magma with higher concentrations of U and HREEs cannot fully explain the difference between measured and calculated results, because perovskite has strong preference for Th (D_{Th} = 155) and LREEs (D_{La} = 27.9) and exhibits high D_{Th}/D_U (up to 23) and D_{La}/D_{Lu} (up to 14.7) during the crystallization from katungite magma (Chakhmouradian et al., 2013). A likely explanation is that the perovskite/melilitite trace element partitioning was affected by melt structure. Compared with a pure silicate magmatic system, perovskite crystallizing from a carbonatite or a hybrid carbonate-silicate magma would have much lower D_{Th}/D_U (0.57–9.23) and D_{La}/D_{Lu} (0.68–6.25) (Beyer et al., 2013). The low Th/U and La/Yb in the analyzed perovskites thus argue for crystallization from a CO_2-rich primitive melilitite magma.

Perovskite Sr-Nd Isotopic Insights into the Petrogenesis of Melilitites

The early-crystallizing perovskites can better preserve isotopic signatures of the primary magma than the bulk-rock compositions (Tappe et al., 2012; Sun et al., 2014). In

DOI:10.1130/G45329.1

situ Sr-Nd isotopic analyses indicate that most perovskites display lower $^{87}Sr/^{86}Sr_i$ and slightly higher $\varepsilon_{Nd}(t)$ than the melilitite and entrained mantle xenoliths (Fig. 3). The Sr-Nd isotopic variations in mantle-derived rocks may result from source heterogeneities or reflect contamination/alteration during magmat ascent and eruption. The entrainment of various peridotite xenoliths provides convincing evidence for the incorporation of mantle materials into the melilitite magma during ascent through the mantle lithosphere (SCLM) (cf. Su et al., 2012). We modeled the possible assimilation and fractional crystallization (AFC) processes and found that the scatter of bulk-rock Sr-Nd isotopes in the melilitite, as well as their isotopic overlap with mantle xenoliths, can be fully reproduced by incorporating isotopically enriched components from the SCLM (e.g., carbonate- and phlogopite-rich metasomes) into primary melts (in Fig. 3). In this case, the high $^{87}Sr/^{86}Sr_i$ and low $\varepsilon_{Nd}(t)$ observed in some perovskite grains (e.g., LX1506@12) can be best explained as reflecting the chemical interaction between the primary melilitite magma and the metasomatized SCLM. The discrepancy between in situ perovskite data and bulk-rock isotopic compositions thus underscores the potential of early-crystallizing perovskites to probe into the nature of mantle sources and also corroborates the inevitable contamination/assimilation of primary melilitite magma during ascent.

A common characteristic for perovskites from the West Qinling melilitite and Group I kimberlites worldwide is their comparable Sr-Nd isotopic co-variations that overlap with the variation range of modern ocean island basalts (OIBs) and form arrays extending toward the depleted mantle (Fig. 3). Hence both the heterogeneous SCLM and depleted mantle asthenosphere are possible source regions for generating the primary melilitite magma. However, the entrained mantle xenoliths permit direct insights into the SCLM beneath the northeastern Tibetan Plateau (Su et al., 2012). The pronounced difference in Pb isotopic compositions between the melilitite ($^{206}Pb/^{204}Pb$ = 18.088–19.441) and mantle xenoliths ($^{206}Pb/^{204}Pb$ = 16.083–18.020) (Fig. DR6) thus argue against a derivation from partial melting of the SCLM. Melting within mantle lithosphere is further challenged by thermobarometric calculation performed on peridotite xenoliths because it places these mantle debris at depths of 65–125 km (Su et al., 2012) and limits the minimum depth at which mantle melting and extraction of incipient melilitite melts have occurred. With respect to the lithospheric thickness beneath the northeastern Tibetan Plateau (100–130 km, Li et al., 2013), the primary melilitite magma should originate at a depth greater than the lithosphere-asthenosphere boundary (LAB).

Given the Permian-Triassic northward subduction of the Ayimaqin-Kunlun-Mianlue Paleo-Tethyan oceanic lithosphere beneath the West Qinling orogenic belt (cf. Dong and Santosh 2016), we propose that the primary melilitite magma must have ultimately derived from low-degree partial melting of subduction-modified asthenosphere. It can be found that addition of minor amounts (<1 %) of carbonate-bearing pelagic sediments to the depleted mantle is sufficient to reproduce the Sr-Nd isotopic array defined by the melilititic perovskites (Fig. 3). Such interpretation is compatible with the

OIB-like trace element features (e.g., high Ce/Pb and Nb/U, Fig. DR3) and the radiogenic Pb isotopic compositions (Fig. DR6) shown by the West Qinling melilitite. It is also supported by experimental results in which melilitite melts are generated via small-degree (<1%) melting of CO_2-bearing peridotite (<4 GPa, Gudfinnsson and Presnall, 2005), particularly if the isotopically light Mg in melilitites ($\delta^{26}Mg = -0.54‰$ to $-0.32‰$, Dai et al., 2017) are considered to represent carbonate-related metasomatism in their mantle sources. Together with the Neogene-Quaternary (ultra) potassic rocks in northern Tibet (Guo et al., 2006), it is tenable that multiple episodes of oceanic subduction and continental convergence could have given rise to significant heterogeneities in the upper mantle and consequently contributed to postcollisional alkaline magmatism along the Kunlun fault zone.

Implications for the Northeastward Growth of the Tibetan Plateau

Identification of mantle-derived alkaline magmatism and how it relates to tectonic escape in response to the India-Asia convergence are key to unraveling the outward growth mechanism of the Tibetan plateau (Tapponnier et al., 2001; Wang et al., 2001). Our new perovskite U-Pb ages indicate that the melilitite magmatism is broadly coeval with (ultra) potassic activities on the northern Tibetan Plateau (Fig. 1B), both of which coincide with the onset of Kunlun strike-slip faulting since the early Miocene (Duvall et al., 2013). The linear distribution and long temporal span (~25 Myrs) of these postcollisional magmatic rocks (Fig. 1) argue against a rapid removal of SCLM beneath

DOI:10.1130/G45329.1

the northern Tibet. Because seismic tomography shows a low-velocity dome right beneath the Kunlun fault zone at depth of 90–150 km (Fig. 4), an alternative explanation is that these volumetrically small alkaline rocks may be formed via decompression melting of mantle asthenosphere and emplaced along narrow conduits of Kunlun fault zone. For the melilitite on the northeastern Tibetan Plateau, carbonatite metasomatism would dramatically lower the solidus temperature in their mantle sources and facilitate mantle melting (Gudfinnsson and Presnall, 2005). Meanwhile, the deeply rooted Kunlun fault system, which propagates along the weakly welded AKMS (Fig. 1A) and cuts through the entire lithosphere (Li et al., 2013), would provide magmatic pathways and allow such volatile-rich magma to migrate rapidly to the surface.

Given that the continued India-Asia convergence would reactivate pre-existing zones of weakness in the Asian lithosphere away from the collision zone (Tapponnier et al., 2001), the highly localized decompression melting of refertilized mantle asthenosphere may also explain the formation of alkaline magmatism along Ailao Shan-Red River shear zone (Wang et al., 2001) and Karakorum-Shigar strike-slip fault zone (Mahéo et al., 2009). Therefore, our perovskite U-Pb dating results not only provide a time constraint on the initiation of the Kunlun strike-slip faulting and associated tension gash, but also highlight the controlling role of pre-existing lithospheric weakness in intracontinental deformation, tectonic extrusion, and emplacement of postcollisional magmatism accompanying the outward plateau growth.

CONCLUSIONS

The textural and geochemical features of the perovskite crystals are consistent with their early crystallization from a CO_2-rich melilitite magma. The moderately depleted Sr-Nd isotopic signatures in these perovskites, as well as the OIB-like characteristics shown by the West Qinling melilitite, indicate that their primary magma could originate from the low-degree partial melting of refertilized asthenosphere. Perovskite U-Pb dating results corroborate the temporal correlation between the melilitite magmatism and the Kunlun strike-slip faulting. The generation of volumetrically small mantle-derived alkaline magmatism along major strike-slip faults can be best interpreted as resulting from partial melting of metasomatized asthenosphere induced by the reactivation of trans-lithospheric shear zones.

ACKNOWLEDGMENTS

We thank Chris Clark for editorial handling, and Jörn-Frederik Wotzlaw, Catherine Mottram, and Sebastian Tappe for insightful comments. We are grateful to Yue-Heng Yang, Qiu-Li Li, Xiao-Xiao Ling, and Qian Ma for assistance with in situ analysis. This study was supported by the China 973 Program (project 2015CB452604), the Natural Science Foundation of China (grant 41802058), and the 111 project (B18048).

REFERENCES CITED

Beyer, C., Berndt, J., Tappe, S., and Klemme, S., 2013, Trace element partitioning between perovskite and kimberlite to carbonatite melt: New experimental constraints:

Chemical Geology, v. 353, p. 132–139, https://doi.org/10.1016/j.chemgeo.2012.03.025.

Chakhmouradian, A.R., Reguir, E.P., Kamenetsky, V.S., Sharygin, V.V., and Golovin, A.V., 2013, Trace-element partitioning in perovskite: implications for the geochemistry of kimberlites and other mantle-derived undersaturated rocks: Chemical Geology, v. 353, p. 112–131, https://doi.org/10.1016/j.chemgeo.2013.01.007.

Dai, L.-Q., Zhao, Z.-F., Zheng, Y.-F., An, Y.-J., and Zheng, F., 2017, Geochemical Distinction between Carbonate and Silicate Metasomatism in Generating the Mantle Sources of Alkali Basalts: Journal of Petrology, v. 58, p. 863–884, https://doi.org/10.1093/petrology/egx038.

Dong, Y., and Santosh, M., 2016, Tectonic architecture and multiple orogeny of the Qinling Orogenic Belt, Central China: Gondwana Research, v. 29, p. 1–40, https://doi.org/10.1016/j.gr.2015.06.009.

Duvall, A.R., Clark, M.K., Kirby, E., Farley, K.A., Craddock, W.H., Li, C., and Yuan, D.Y., 2013, Low-temperature thermochronometry along the Kunlun and Haiyuan Faults, NE Tibetan Plateau: Evidence for kinematic change during late-stage orogenesis: Tectonics, v. 32, p. 1190–1211, https://doi.org/10.1002/tect.20072.

Gudfinnsson, G.H., and Presnall, D.C., 2005, Continuous gradations among primary carbonatitic, kimberlitic, melilititic, basaltic, picritic, and komatiitic melts in equilibrium with garnet lherzolite at 3–8 GPa: Journal of Petrology, v. 46, p. 1645–1659, https://doi.org/10.1093/petrology/egi029.

Guo, Z., Wilson, M., Liu, J., and Mao, Q., 2006, Post-collisional, potassic and ultrapotassic magmatism of the northern Tibetan Plateau: Constraints on characteristics of the mantle source, geodynamic setting and uplift mechanisms: Journal of Petrology, v. 47, p. 1177–1220, https://doi.org/10.1093/petrology/egl007.

Li, L., Li, A., Shen, Y., Sandvol, E.A., Shi, D., Li, H., and Li, X., 2013, Shear wave structure in the northeastern Tibetan Plateau from Rayleigh wave tomography: Journal of Geophysical Research. Solid Earth, v. 118, p. 4170–4183, https://doi.org/10.1002/jgrb.50292.

Mahéo, G., Blichert-Toft, J., Pin, C., Guillot, S., and Pêcher, A., 2009, Partial Melting of Mantle and Crustal Sources beneath South Karakorum, Pakistan: Implications for the Miocene Geodynamic Evolution of the India-Asia Convergence Zone: Journal of Petrology, v. 50, p. 427–449, https://doi.org/10.1093/petrology/egp006.

Molnar, P., England, P., and Martinod, J., 1993, Mantle dynamics, uplift of the Tibetan Plateau, and the Indian monsoon: Reviews of Geophysics, v. 31, p. 357–396, https://doi.org/10.1029/93RG02030.

Su, B.-X., Zhang, H.-F., Ying, J.-F., Tang, Y.-J., Hu, Y., and Santosh, M., 2012, Metasomatized lithospheric mantle beneath the western Qinling, Central China: insight into carbonatite melts in the mantle: The Journal of Geology, v. 120, p. 671–

681, https://doi.org/10.1086/667956.

Sun, J., Liu, C.-Z., Tappe, S., Kostrovitsky, S.I., Wu, F.-Y., Yakovlev, D., Yang, Y.-H., and Yang, J.-H., 2014, Repeated kimberlite magmatism beneath Yakutia and its relationship to Siberian flood volcanism: Insights from in situ U–Pb and Sr–Nd perovskite isotope analysis: Earth and Planetary Science Letters, v. 404, p. 283–295, https://doi.org/10.1016/j.epsl.2014.07.039.

Sun, S.S., and McDonough, W.F., 1989, Chemical and isotopic systematics of oceanic basalts: implications for mantle composition and processes: Geological Society of London, Special Publications, v. 42, p. 313–345, https://doi.org/10.1144/GSL.SP.1989.042.01.19.

Tappe, S., Steenfelt, A., and Nielsen, T., 2012, Asthenospheric source of Neoproterozoic and Mesozoic kimberlites from the North Atlantic craton, West Greenland: new high-precision U–Pb and Sr–Nd isotope data on perovskite: Chemical Geology, v. 320, p. 113–127, https://doi.org/10.1016/j.chemgeo.2012.05.026.

Tapponnier, P., Xu, Z., Roger, F., Meyer, B., Arnaud, N., Wittlinger, G., and Yang, J., 2001, Oblique stepwise rise and growth of the Tibet plateau: Science, v. 294, p. 1671–1677, https://doi.org/10.1126/science.105978.

Wang, C., Dai, J., Zhao, X., Li, Y., Graham, S.A., He, D., Ran, B., and Meng, J., 2014, Outward-growth of the Tibetan Plateau during the Cenozoic: A review: Tectonophysics, v. 621, p. 1–43, https://doi.org/10.1016/j.tecto.2014.01.036.

Wang, J.-H., Yin, A., Harrison, T.M., Grove, M., Zhang, Y.-Q., and Xie, G.-H., 2001, A tectonic model for Cenozoic igneous activities in the eastern Indo–Asian collision zone: Earth and Planetary Science Letters, v. 188, p. 123–133, https://doi.org/10.1016/S0012-821X(01)00315-6.

Yang, Y.-H., Wu, F.-Y., Wilde, S.A., Liu, X.-M., Zhang, Y.-B., Xie, L.-W., and Yang, J.-H., 2009, In situ perovskite Sr–Nd isotopic constraints on the petrogenesis of the Ordovician Mengyin kimberlites in the North China Craton: Chemical Geology, v. 264, p. 24–42, https://doi.org/10.1016/j.chemgeo.2009.02.011.

FIGURE CAPTIONS

Figure 1. (A) Topographic map of northeastern Tibetan plateau, showing tectonic framework and spatial distribution of postcollisional magmatism along the Kunlun fault. AKMS = Ayimaqin-Kunlun-Mutztagh suture zone, JSS = Jinsha suture zone, BNS = Bangong-Nujiang suture zone; ATF = Altyn Tagh fault, HF = Haiyuan fault, KLF = Kunlun fault, WQF = West Qinling fault; LST = Liupan Shan thrust belt, QS-NST = Qilian Shan-Nan Shan thrust belt, QTT = Qimen Tagh thrust belt. The Cenozoic basins in northeastern Tibet were denoted by gray areas. (B) Variation in the formation ages of melilitites, shoshonites, and (ultra) potassic rocks along the Kunlun fault (Table DR1 in the GSA Data Repository[1]).

DOI:10.1130/G45329.1

Figure 2. Primitive mantle (values from Sun and McDonough, 1989) normalized trace element patterns of melilititic perovskites. Trace element patterns of kimberlitic perovskites (Yang et al., 2009; Sun et al., 2014) are shown for comparison.

Figure 3. Initial Sr-Nd isotopic compositions of perovskites, melilitites, and mantle xenoliths. The labeled percentages along AFC modeling and binary mixing curves denote the increments of SCLM metasomes and recycled sediments, respectively. D_{Sr} (0.6) and D_{Nd} (0.2) were estimated by assuming cumulates of pyroxene + plagioclase + olivine + phlogopite + perovskite, and R value was set to be 0.99. Details of geochemical end-members were given in Table DR8. Data field of mid-ocean ridge basalts (MORBs) and OIBs (*http://georoc.mpch-mainz.gwdg.de/georoc/*), kimberlitic perovskites (Tappe et al., 2012; Sun et al., 2014), and (ultra) potassic rocks in northern Tibet (Guo et al., 2006) are shown for comparison.

Figure 4. Topographic and seismic profiles across northeastern Tibet in the NE-SW direction (Li et al., 2013), showing a shear wave velocity perturbation beneath the Kunlun fault zone. Arrows denote the possible escape flow and the upward migration trend of asthenospheric melts along Kunlun fault system.

1GSA Data Repository item 2018xxx, method description and analytical results (Tables DR1-DR8 and Figure DR1-DR7), is available online at

DOI:10.1130/G45329.1

http://www.geosociety.org/datarepository/2018/, or on request from editing@geosociety.org.

Liu et al. Fig. 1 W175 mm - H62 mm (3-column fitting image)

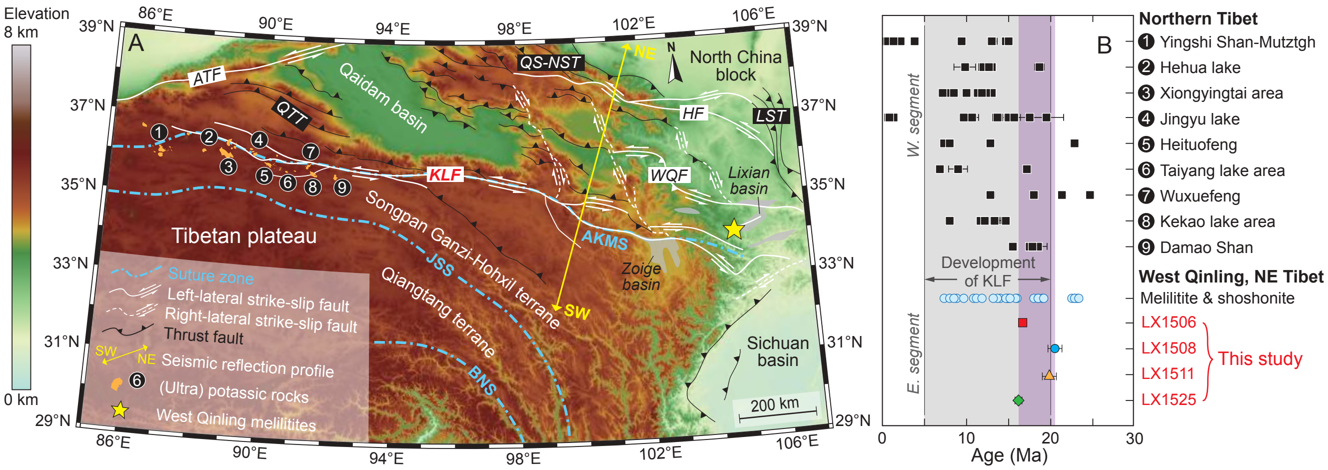

Liu et al. Fig. 2 W58 mm - H41 mm (1-column fitting image)

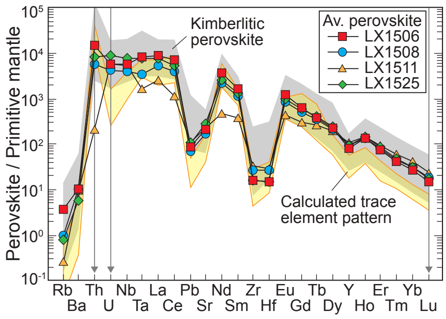

Liu et al. Fig. 3 W58 mm - H73 mm (1-column fitting image)

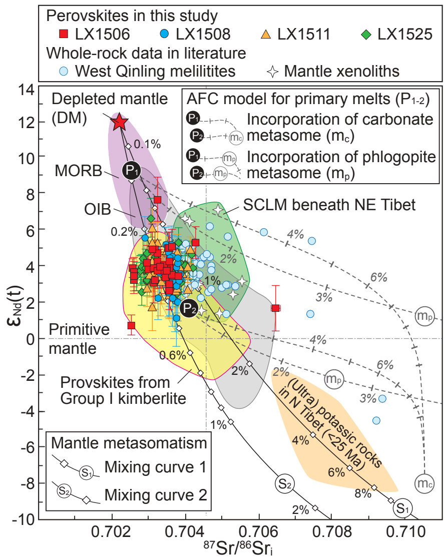

Liu et al. Fig. 4 W58 mm - H40 mm (1-column fitting image)

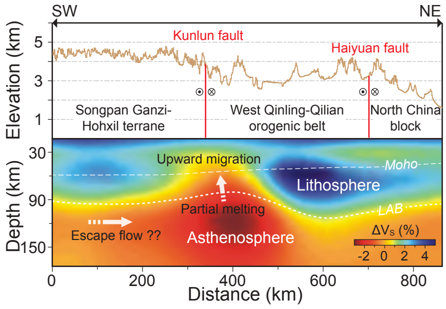

GSA Data Repository 2018XXX

Perovskite U-Pb and Sr-Nd isotopic perspectives on kamafugitic magmatism and northeastward growth of the Tibetan plateau

Dong Liu* *et al.*

* Corresponding author, E-mail: d.liu@cugb.edu.cn

Contents

Analytical methods

Major and trace element analyses of west Qinling kamafugites

Major and trace element analyses were conducted in the State Key Laboratory of Geological Processes and Mineral Resources (GPMR), China University of Geosciences at Wuhan. Analytical results of kamafugite samples, procedural blanks, and international standards were given in Table DR2.

Weathered rock surfaces have been removed before analysis. After extracting mantle xenoliths by handpicking, fresh kamafugite samples were powdered into 200 mesh. Rock powder (~0.5 g) was mixed with 5.0 g compound flux ($Li_2B_4O_7$: $LiBO_2$ = 12 : 22), and then was fused in a Pt-Au crucible by heating at ~1050°C for 11 min. The mixture was swirled repeatedly to ensure complete dissolution and homogenization before pouring into a mold to form a flat-surfaced disc (34 mm in diameter) for further analysis. Major element analysis was conducted using a *Shimadzu XRF-1800* sequential X-ray fluorescence spectrometry. Sample-preparing procedures and operating conditions of the XRF instrument have been described by Ma et al. (2012). The precision and accuracy for major element data are better than 4% and 3%, respectively.

As for trace element analysis, rock powder (~50 mg) was dissolved in a Teflon bomb with HF + HNO_3 mixture, and then was heated at 190°C for 48 h. After evaporating the solution to dryness, the dried sample was re-dissolved using ~3 ml 30% HNO_3, and then heated at 190°C for 24 h. Final solution was diluted to ~100 g with 2% HNO_3 for subsequent analysis. Trace element analysis was conducted using an *Agilent 7500a* inductively coupled plasma-mass spectrometry (ICP-MS). Detailed operating conditions of the ICP-MS instrument and data reduction processes have been described by Liu et al. (2008).

Major and trace element analyses of perovskites

Fresh kamafugite samples were crushed to 80 mesh, and then perovskites extracted from the crushed kamafugites were mounted in epoxy resin and polished to expose grain interiors. Back-scattered electron (BSE) images and major element compositions of perovskites were conducted using a *JEOL-JAX8100* electron microprobe with accerlerating voltage of 15 kV and beam current of 12 nA. Trace element compositions of perovskites were conducted using an *Agilent 7500a* ICP-MS equipped with a 193 nm excimer ArF laser-ablation system (*GeoLas Plus*) at the Institute of Geology and Geophysics, Chinese Academy of Sciences (IGG-CAS). Helium gas was flushed to minimize aerosol deposition around the ablation site, and mixed with argon gas downstream of the ablation cell. The diameter of spot size was 40 µm. The repetition rate of 8 Hz and the laser energy density of 12.9 J/cm^2 were used in this study. Every ten sample analyses were followed by analyzing one NIST 610 and NIST 612 glasses. Each analysis incorporated a background acquisition of approximately ~20 s (gas blank) and ~40 s sample data acquisition. Trace element concentrations were calculated using *GLITTER 4.0* software (Griffin et al., 2008), and calibrated against NIST 610 as an external standard combined with isotope ^{43}Ca (based on CaO concentration measured by electron probe) as an internal standard. Major and trace element data of perovskite samples were given in Table DR3.

In situ U-Pb dating

Perovskite U-Pb dating were conducted using a CAMECA IMS-1280 secondary ion mass spectrometry (SIMS) at the IGG-CAS. The O^{2-} primary ion beam was accelerated at 13 kV, with an intensity ranging from 9 nA to 14 nA. Positive secondary ions were extracted by a potential of 10 kV. The ellipsoidal spot was about 20 × 30 µm in size.

In this study, perovskites mounted in epoxy resin was coated with 30 nm high purity gold to reach 20 Ω resistance. Sample charging effects were minimized by optimizing the energy offset to maximum transmission in an energy window of 60 eV at the start of each analysis, using the $^{40}Ca^{48}Ti_2{}^{16}O_4$ reference peak at mass 200. A mass resolution of ~7000 (defined at 50% peak height) was used to separate $^{40}Ca^{48}Ti_2{}^{16}O_4{}^{+}$ peaks from isobaric interferences (Li et al., 2010), which was enough to separate U, Th, and Pb isotopes from isobaric interferences (e.g. oxides of REE, Williams, 1998). A single electron multiplier was used in the ion-counting mode to measure secondary ion beam intensities by peak jumping sequence. Each measurement consists of 10 cycles, and total data acquisition time is ~12 min. Analytical method and detailed operating conditions for the CAMECA IMS-1280 has been described by Li et al. (2010).

Given that perovskite commonly contains significant amounts of common Pb, we plotted the common Pb uncorrected data on the Tera-Wasserburg concordia diagram to obtain the crystallization age of the analyzed perovskites from the lower intercept. The upper intercept was fixed assuming that the initial common lead isotope composition follows the terrestrial Pb isotope evolution model described by Stacey and Kramers (1975) (i.e. the SK model Pb isotopes). Besides, the ^{207}Pb correction method was also applied for individual analysis, and average $^{206}Pb/^{238}U$ ages were calculated using ISOPLOT 3.0 (Ludwig, 2003).

Perovskite Tazh-3 was used as the primary standard (Kinny et al., 1997) to calibrate U-Th-Pb data, and every five or six sample analyses was followed by analyzing a Tazh-3 standard.

The in-house AFK perovskite standard was analyzed as an unknown during each analytical session, and yielded a lower intercept age of 379.0 ± 2.9 Ma (MSWD = 1.20) and a weighted average $^{206}Pb/^{238}U$ age of 379.1 ± 3.2 Ma (MSWD = 1.06, n = 17) (Fig. DR6), both of which are consistent with the recommended age of 381.6 ± 1.4 Ma (Wu et al., 2013). The SIMS U-Pb isotopic data of perovskite samples and standard were given in Table DR4.

In situ analysis of Sr-Nd isotopes

In situ Rb-Sr and Sm-Nd isotopic analyses on perovskites were conducted using a *Neptune* multi-collector (MC)-ICPMS at the IGG-CAS. The detailed operating conditions for MC-ICPMS instrument, the isotopic measurements, and the data reduction processes have been described by Yang et al. (2009) and Wu et al. (2010). Possible isobaric interferences and their correction methods were reported by Ramos et al. (2004) and have been successfully applied in Yang et al. (2009). Therefore, a brief description is given below.

The Sr isotopic data were obtained in a static multi-collector mode with a low resolution using nine Faraday collectors and the mass configuration array from ^{83}Kr to ^{88}Sr aimed at monitoring Kr and Rb (Ramos et al., 2004; Yang et al., 2009). During Sr isotopic analysis, an aliquot of 200 ppb NIST SRM 987 standard solution was used for controlling the quality and optimizing the operation parameters (including torch position, Ar flow rate, and ion lens focus) to get maximum sensitivity. The *Neptune* MC-ICPMS was configured to monitor Kr in the Ar gas after optimization prior to each analytical session (Yang et al., 2009). The spot size was 32-44 μm in this study, with a pulse rate of 8 Hz and a laser energy density of 10 J/cm^2. During each analysis, a 30-second measurement of the gas blank was carried out prior to ablation in order to correct Kr (Ramos et al., 2004). The natural Kr ratios, including $^{83}Kr/^{84}Kr$ of 0.20175 and $^{83}Kr/^{86}Kr$ of 0.66474, were used for overlap correction, and the $^{85}Rb/^{87}Rb$ of 2.5926 was used for isobaric correction of Rb through exponential law (Ehrlich et al., 2001). Note that the perovskite samples in this study commonly have extremely low Rb/Sr ratios (< 0.002, Table DR3), the small fraction of Rb in the Sr fraction can be effectively corrected (Yang et al., 2009). No correction was applied for the interference from Fe dioxides, Ga and Zn oxides were negligible because of their low signals (Yang et al., 2009). However, interference from the doubly-charged rare earth elements can not be ignored because of their high concentrations in perovskite. The contributions of $^{168}Er^{2+}$ and $^{168}Yb^{2+}$ to ^{84}Sr, $^{170}Er^{2+}$ and $^{170}Yb^{2+}$ to ^{85}Rb, $^{172}Yb^{2+}$ to ^{86}Sr, $^{174}Yb^{2+}$ to ^{87}Sr (+^{87}Rb), and $^{176}Yb^{2+}$ to ^{88}Sr were calculated according to the isotopic abundances of Er and Yb (Ramos et al., 2004). In this study, the analyzed perovskite samples are characterized by low Er/Sr (< 0.015) and Yb/Sr (< 0.007) (Table DR3), indicating that the interferences can be effectively corrected. On the other hand, the interferences of $^{176}Lu^{2+}$ and $^{176}Hf^{2+}$ on ^{88}Sr are negligible due to their low signals during in situ analysis (Ramos et al., 2004; Yang et al., 2009). The AFK perovskite standard was used as the external standard in this study, yielding an average $^{87}Sr/^{86}Sr$ of 0.703345 ± 0.000144 (2σ, n = 49, Fig. DR6), which agreed well with the recommended value within 2σ error ($^{87}Sr/^{86}Sr$ = 0.703347 ± 0.000039, Wu et al., 2013). The Rb-Sr isotopic data of perovskite samples and standard were given in Table DR5.

The in situ Sm-Nd isotopic data were obtained using an anlytical method similar to the Rb-Sr isotope determinations described above. The La Jolla Nd standard solution was used for instrumental calibration, and the exponential law was applied for mass bias correction by assuming $^{146}Nd/^{144}Nd$ of 0.7219. Because the studied perovskites are enriched in REEs and have high concentrations of Nd (up to 5596 ppm, Table DR3), in situ Sm-Nd isotope data can be obtained using a spot size of 32-60 μm, with the pulse rate of 5-8 Hz and the laser energy density of 10-11 J/cm^2. The influence of Ce on Nd isotopic analysis was proved to be negligible (Yang et al., 2009), suggesting that sufficient attention must be paid to the isobaric interference of ^{144}Sm on ^{144}Nd (McFarlane and McCulloch, 2007). The mass bias of Sm (β_{Sm}) value directly obtained from the $^{147}Sm/^{149}Sm$ ratio of sample itself in real-time was applied to isobaric interference correction following the method proposed by McFarlane and McCulloch (2007). The $^{147}Sm/^{149}Sm$ of 1.08680 (Dubois et al., 1992) and the $^{144}Sm/^{149}Sm$ of 0.22332 (Isnard et al., 2005) were used for data reduction, and the $^{145}Nd/^{144}Nd$ ratio, with a constant value of 0.348415 (Wasserburg et al., 1981), was used to evaluate the effectiveness of analytical method. The AFK perovskite standard was used for external corrections of $^{147}Sm/^{144}Nd$ and $^{143}Nd/^{144}Nd$ in this study, yielding average $^{143}Nd/^{144}Nd$ of 0.512605 ± 0.000037 (2σ, n = 51, Fig. DR6). These results agree with the recommended values within 2σ error ($^{143}Nd/^{144}Nd$ = 0.512609 ± 0.000027, Wu et al., 2013).

Initial $^{143}Nd/^{144}Nd$ ratios and $\varepsilon_{Nd}(t)$ values were calculated with reference to the chondritic reservoir (CHUR) at the time of perovskites growth from magma. In situ Sm-Nd isotopic data, detailed calculation formulas, and decay constant used in this work were given in Table DR6.

Liu et al.'s Figure DR1

(A-D) Field occurrence for kamafugites and extrusive carbonatites at west Qinling.
(E-H) Photomicrographs for the studied kamafugite samples. Carb = carbonate, Cpx = clinopyroxene, Ol = olivine, Opx = orthopyroxene, Prv = perovskite.

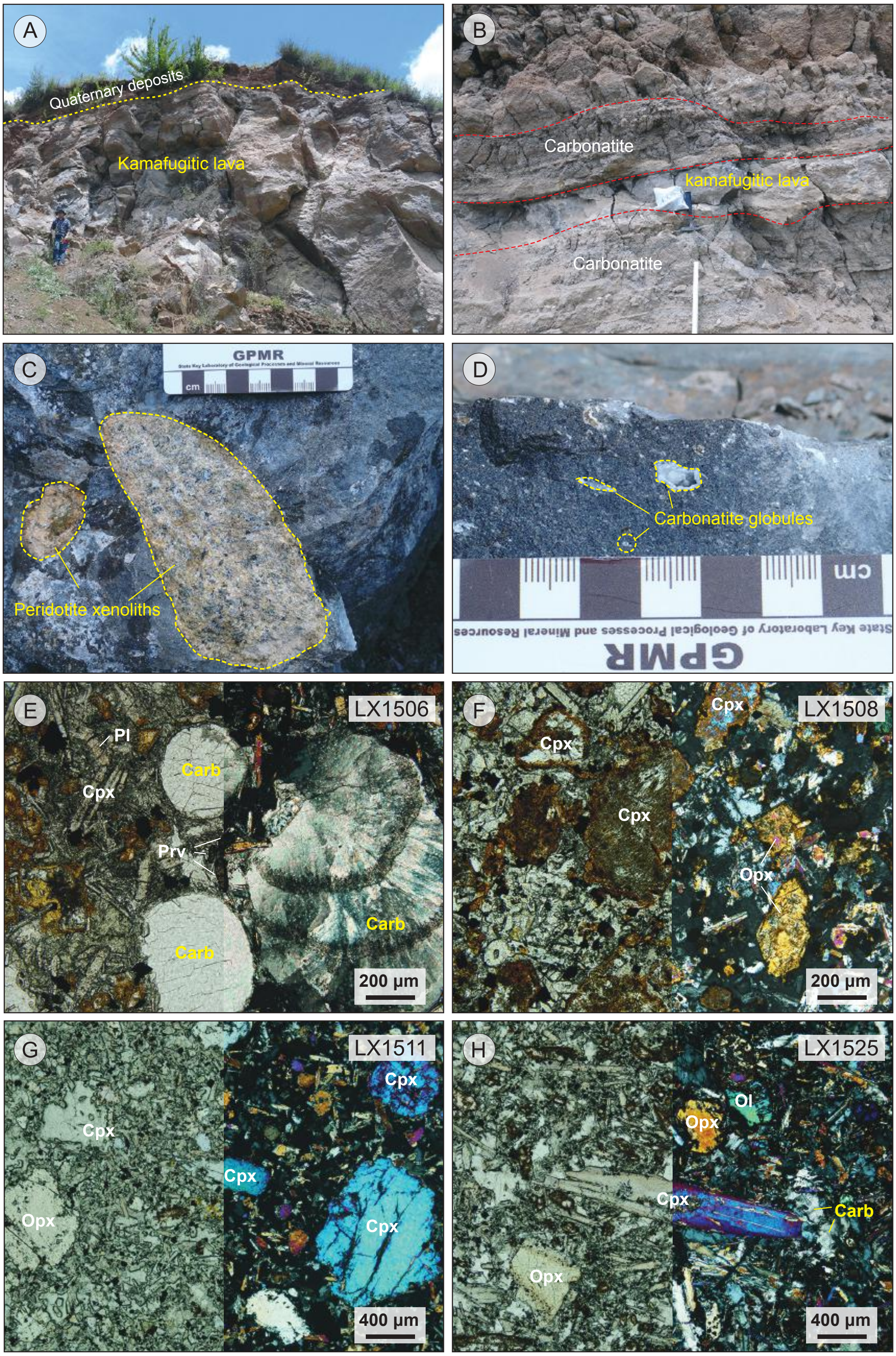

Liu et al.'s Figure DR2

(A) Total alkalis vs. SiO_2 classification diagram (Le Maitre, 2002) for the west Qinling kamafugites. Data field of kamafugites from Brazil, Italy, and Uganda are shown for comparison (Guo et al., 2014 and references therein). (B) Classification diagram of melilitite, nephelinitic rocks, and basanite (Le Bas, 1989). (C) K_2O vs. Na_2O diagram for showing the Na_2O-rich signature in west Qinling kamafugites. Major and trace element data of west Qinling kamafugites are from Yu et al. (2001, 2004, 2009), Wang and Li (2003), Stoppa and Schiazza (2013), Guo et al. (2014), and Dai et al. (2017). (D) Primitive mantle-normalized incompatible trace element distribution patterns for kamafugites.

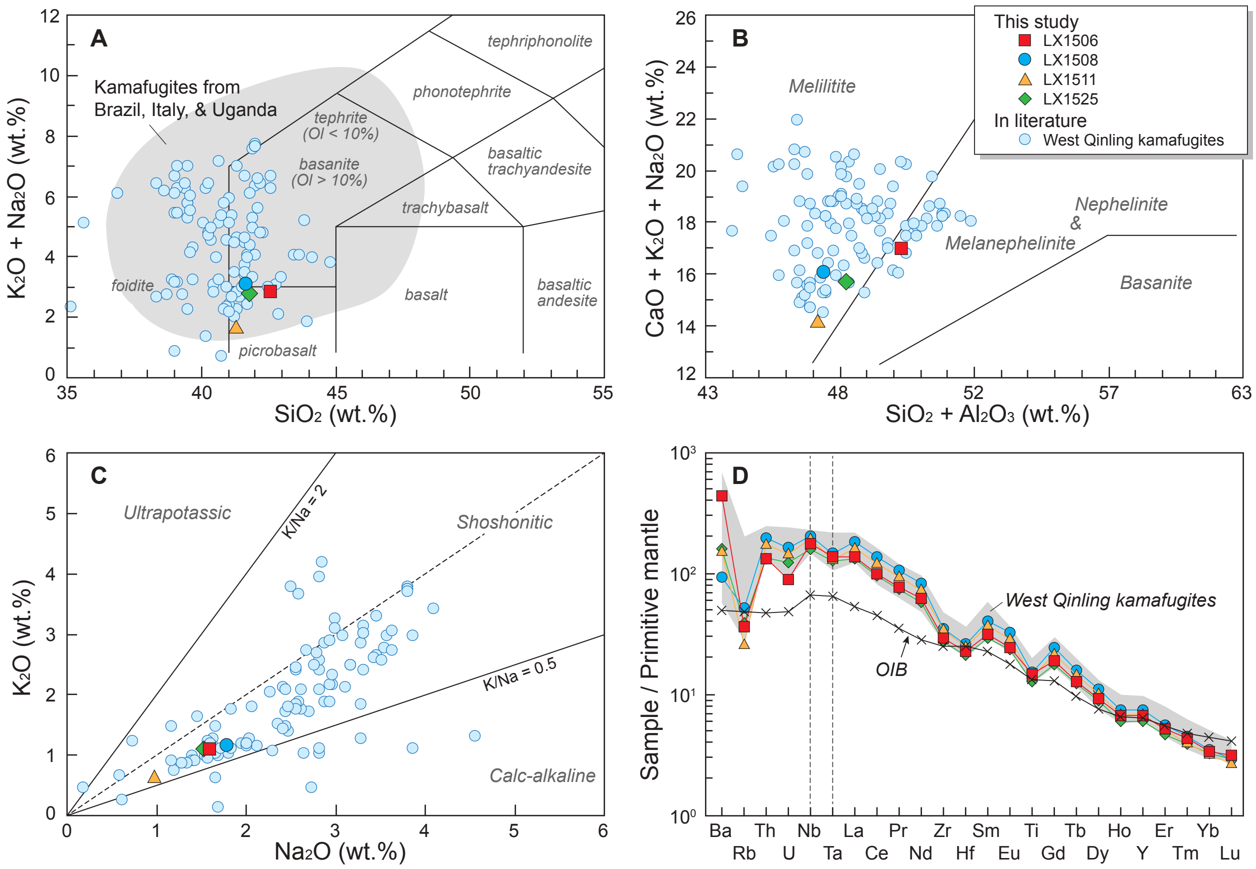

Liu et al.'s Figure DR3

Back-scattered electron (BSE) images for representative perovskites from west Qinling kamafugites. Solid and dashed circles indicate the locations of SIMS U-Pb dating and in situ Sr-Nd isotopic analyses, respectively.

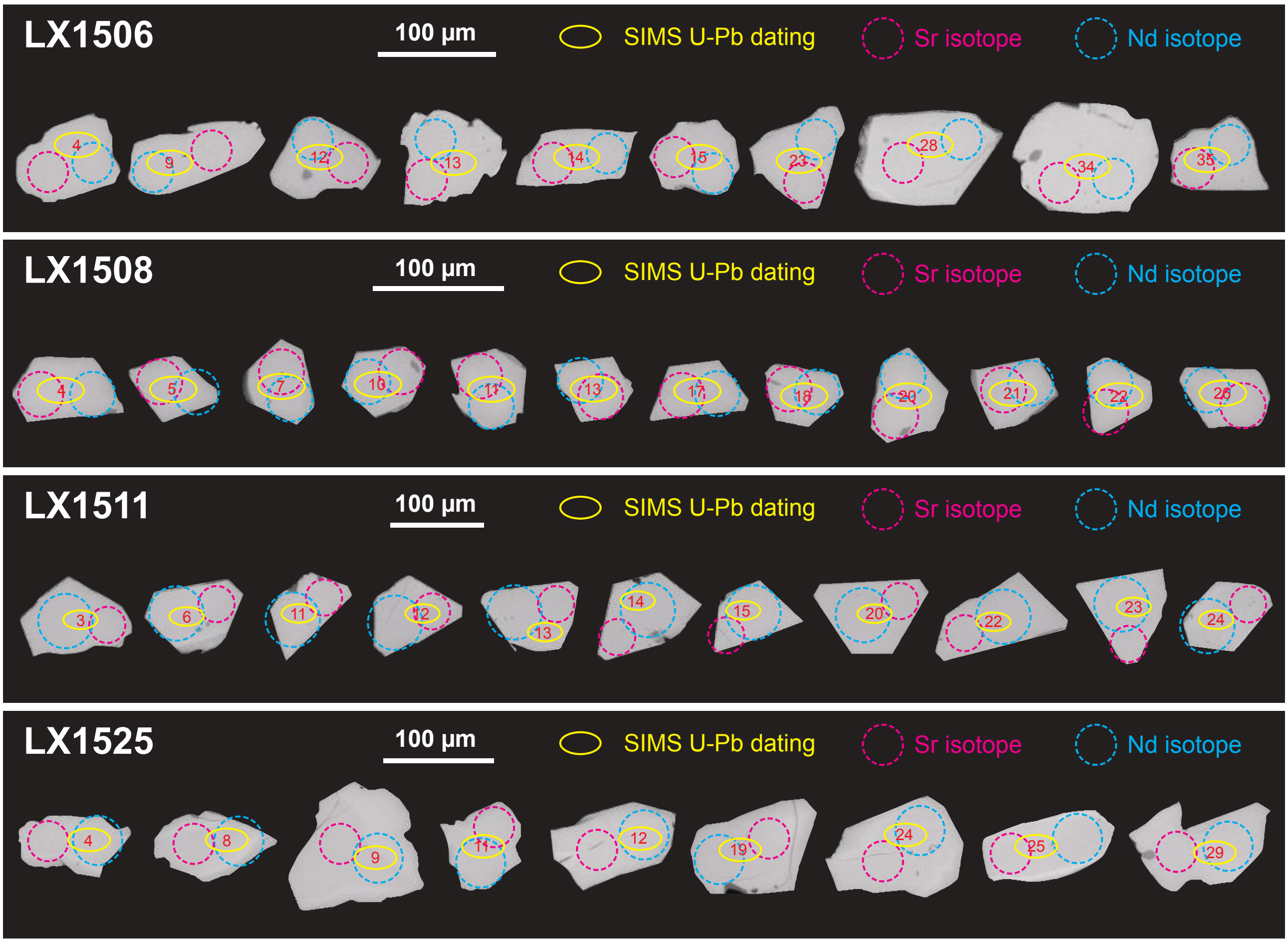

Liu et al.'s Figure DR4

Tera-Wasserburg inverse U-Pb concordia plots and primitive mantle-normalized trace element distribution patterns (Sun and McDonough, 1989) for perovskites from west Qinling kamafugites.

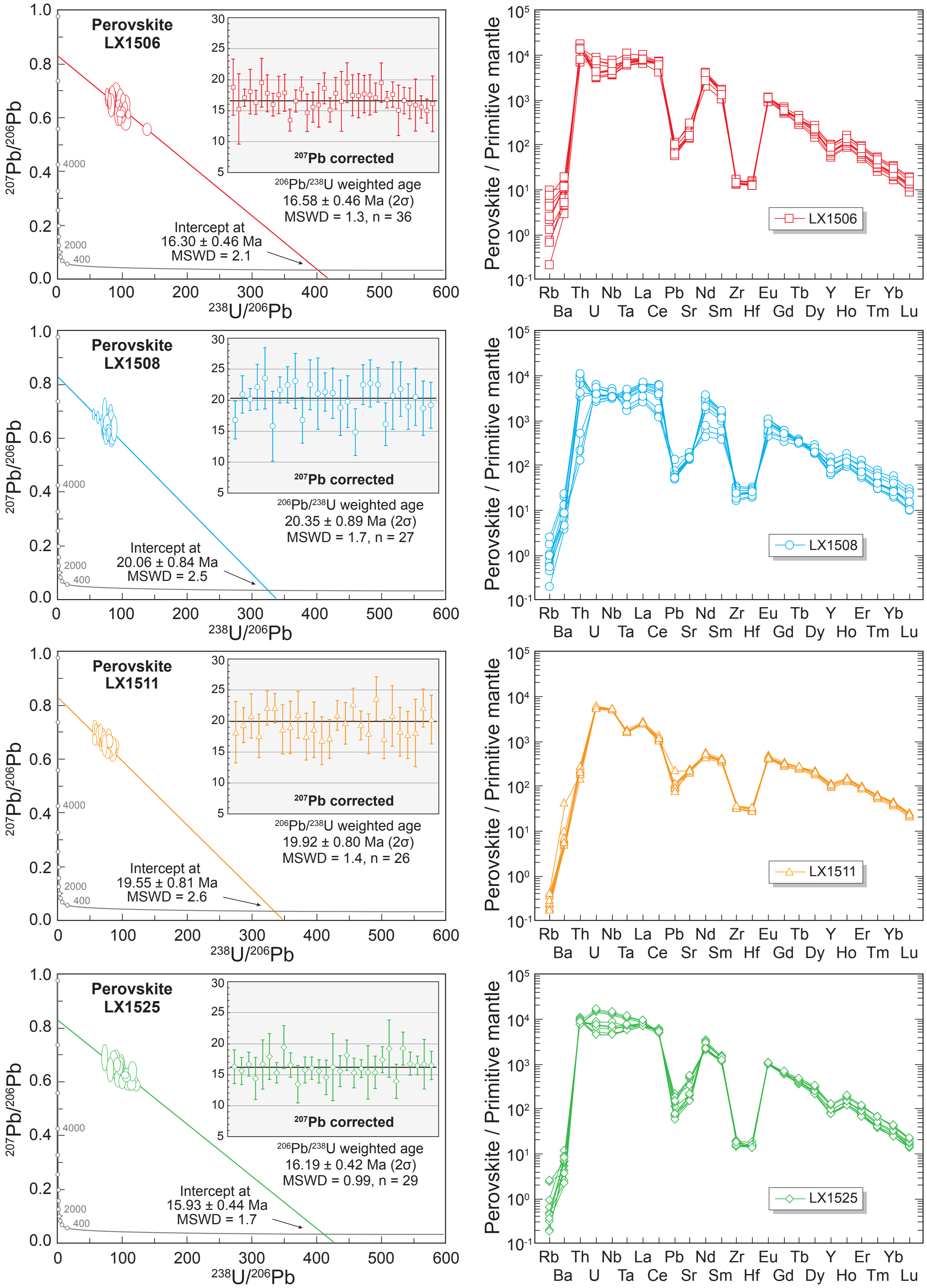

Liu et al.'s Figure DR5

Tera-Wasserburg concordia plot, primitive mantle-normalized trace element distribution patterns (Sun and McDonough, 1989), $^{87}Sr/^{86}Sr$ and $^{143}Nd/^{144}Nd$ of perovskite standard AFK. The Sr and Nd isotopic ratios are presented in chronological order, and their error bars represent two standard deviations (2σ).

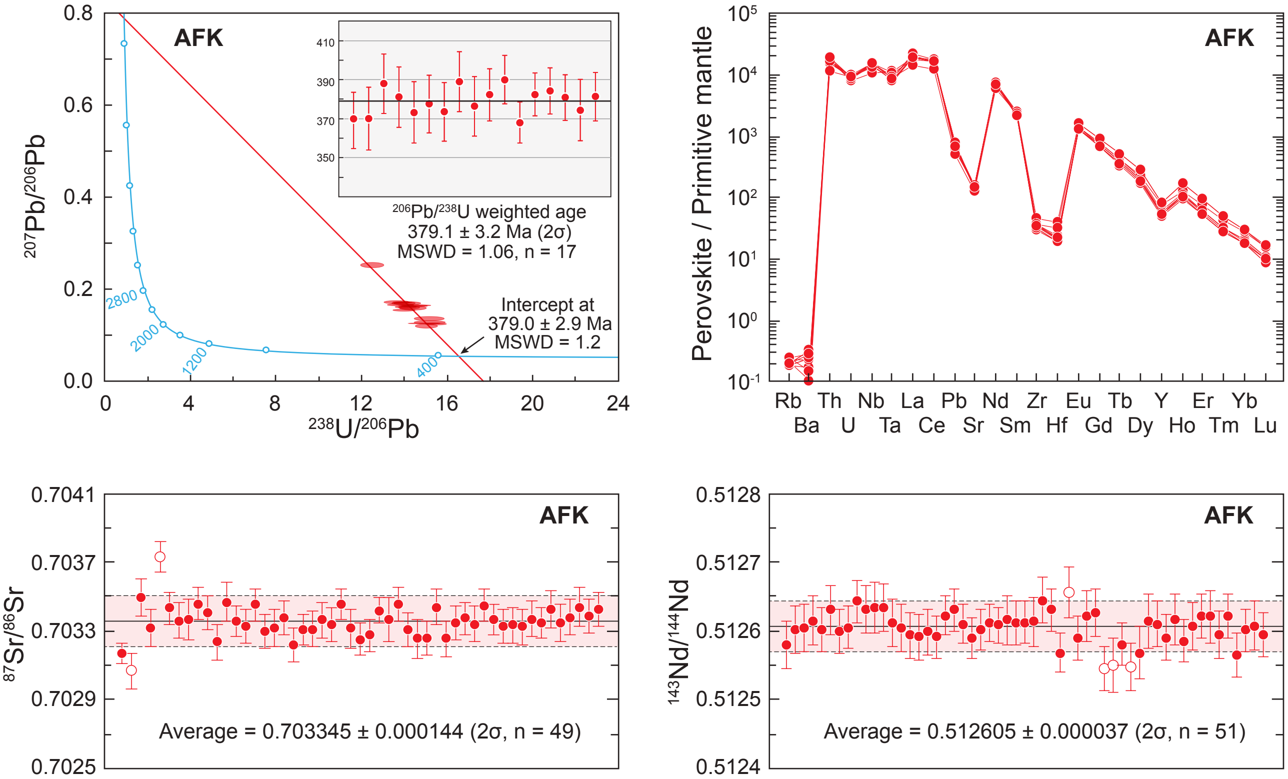

Liu et al.'s Figure DR6

Whole-rock Pb isotopic compositions of the West Qinling kamafugites and the entrained mantle xenoliths. Bulk Silicate Earth (BSE), enriched mantle components (EM I and EM II), prevalent mantle (PREMA), and global subducting sediment (GLOSS) are from Zindler and Hart (1986) and Plank and Langmuir (1998). Northern Hemisphere Reference Line (NHRL): $^{207}Pb/^{204}Pb = 0.1084 \times {}^{206}Pb/^{204}Pb + 13.491$; $^{208}Pb/^{204}Pb = 1.209 \times {}^{206}Pb/^{204}Pb + 15.627$. Isotopic data kamafugites and mantle xenoliths are from Yu et al. (2001, 2004, 2009), Dong et al. (2008), and Su et al. (2012).

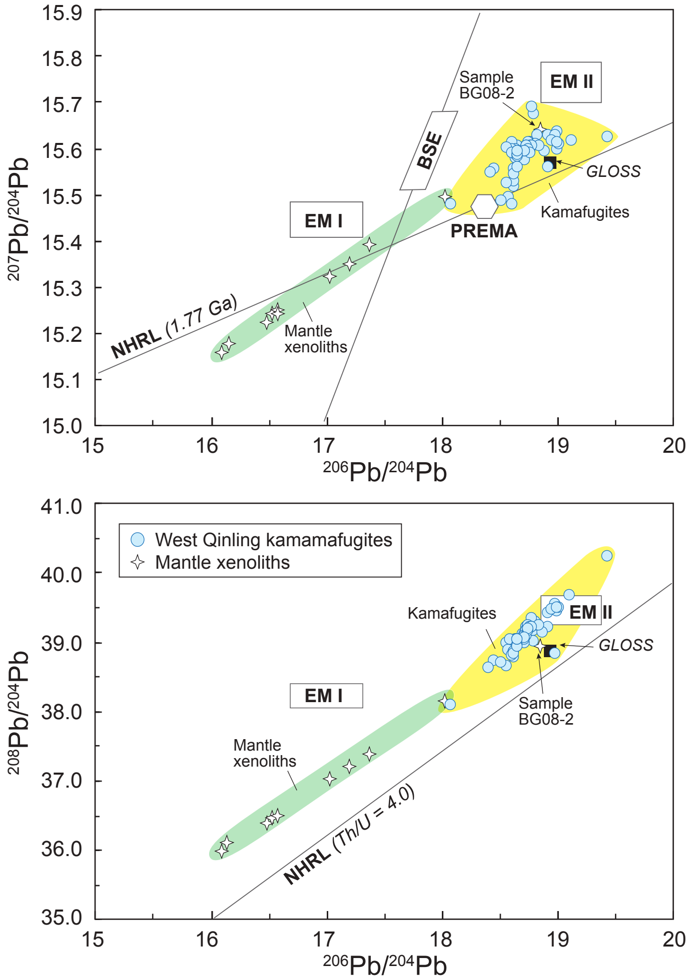

Table DR1 **Ages of the postcollisional magmatic rocks along Kunlun fault system**

No.	Area	Locality	Sample No.	Lithology	Dating method	Age (Ma)	± 2σ	Data source
1	Yingshi Shan -Mutztgh	Canmei Shan	27	Basaltic trachyandesite	WR K-Ar	12.81	0.40	Li et al., 2004
		Canmei Shan	28	Trachyandesite	WR K-Ar	12.85	0.56	Li et al., 2004
		Canmei Shan	36	Trachyte	WR K-Ar	14.51	0.23	Li et al., 2004
		Canmei Shan	169	K-rich Rhyolite	Mus K-Ar	3.65	0.31	Li et al., 2004
		Jinding Shan	1	Andesite	WR K-Ar	0.30	0.07	Li et al., 2004
		Jinding Shan	2	Trachyandesite	WR K-Ar	1.93	0.10	Li et al., 2004
		Jinding Shan	10-1	Basaltic trachyandesite	WR K-Ar	0.45	0.06	Li et al., 2004
		Jinding Shan	43	Trachyandesite	WR K-Ar	1.08	0.07	Li et al., 2004
		Qiangbaqian	-	Trachyandesite	WR K-Ar	14.90		Deng, 1989
		Yurbo Co	-	Trachydacite	WR K-Ar	9.40		Li et al., 1989
2	Hehua lake	Hehua lake	K9024	Trachyandesite	WR Ar-Ar	12.90	0.40	Turner et al., 1996
		Hehua lake	K9026	Trachyandesite	WR Ar-Ar	12.40	0.10	Turner et al., 1996
		Hehua lake	K9028	Basaltic trachyandesite	WR Ar-Ar	18.50	0.60	Turner et al., 1996
		Hehua lake	K9031	Trachyandesite	WR Ar-Ar	11.60	0.10	Turner et al., 1996
		Hehua lake	K9032	Trachyandesite	WR Ar-Ar	11.80	0.20	Turner et al., 1996
		Hehua lake	K9038	Trachyandesite	WR Ar-Ar	9.60	1.30	Turner et al., 1996
		Hehua lake	K9039	Trachyandesite	WR Ar-Ar	12.50	0.30	Turner et al., 1996
3	Xiongyingtai area	Xiongyingtai	K3-3	Latite	WR K-Ar	12.80	0.20	Meng et al., 2002
		Xiongyingtai	K3-11	Shoshonite	WR K-Ar	12.20	0.20	Meng et al., 2002
		Xiongyingtai	K7-34	Shoshonite	WR K-Ar	11.10	0.20	Meng et al., 2002
		Xiangyang lake	HX4-1	Latite	WR K-Ar	7.49	0.17	Deng et al., 1996
		Xiangyang lake	HX4-3	Latite	WR K-Ar	6.95	0.22	Deng et al., 1996
		Xiangyang lake	K9007	Trachyandesite	WR Ar-Ar	11.70	0.30	Turner et al., 1996
		Xiangyang lake	K9016	Trachyte	WR Ar-Ar	8.30	0.10	Turner et al., 1996
		Xiangyang lake	K9018	Trachyte	WR Ar-Ar	9.90	0.30	Turner et al., 1996
4	Jingyu lake	Jingyu lake	AT113	Granite	Ap FT	19.30	1.80	Jolivet et al., 2003
		Jingyu lake	AT118	Granite	Ap FT	17.30	1.80	Jolivet et al., 2003
		Jingyu lake	BJ11	Shoshonite	Ap FT	0.50	0.20	Jolivet et al., 2003
		Jingyu lake	KCS9703b	Shoshonite	Kfs Ar-Ar	14.80	0.61	Jolivet et al., 2003
		Jingyu lake	KCS9704	Shoshonite	Kfs Ar-Ar	9.56	0.34	Jolivet et al., 2003
		Jingyu lake	KCS9708c	Shoshonite	Kfs Ar-Ar	10.57	0.32	Jolivet et al., 2003
		Jingyu lake	KCS9713	Shoshonite	Kfs Ar-Ar	13.27	0.68	Jolivet et al., 2003
		Jingyu lake	J10	Latite	WR K-Ar	0.60	0.06	Yang et al., 2002
		Jingyu lake	J13	Basaltic trachyandesite	WR K-Ar	1.16	0.20	Yang et al., 2002
		Jingyu lake	K2-12	Tephrite	WR K-Ar	0.69	0.12	Yang et al., 2002
		Jingyu lake	K2-29	Latite	WR K-Ar	15.47	0.53	Yang et al., 2002
		Jingyu lake	K2-3-9	Latite	WR K-Ar	13.77	0.34	Yang et al., 2002
		Jingyu lake	K2-3-13	Latite	WR K-Ar	13.53	0.05	Yang et al., 2002
5	Heituofeng	Heituofeng	HX5-3	Latite	WR K-Ar	7.09	0.12	Deng et al., 1996
		Heituofeng	HX5-4	Latite	WR K-Ar	12.60	0.30	Deng et al., 1996
		Heituofeng	KK06038	Trachyte	WR Ar-Ar	7.77	0.26	Jiang et al., 2008
		Heituofeng	GS5035a	Latite	Pl Ar-Ar	22.66	0.11	Zhao et al., 2009
6	Taiyang lake area	Taiyang lake	GS2111a	K-rich rhyolite	Sa Ar-Ar	6.63	0.07	Zhu et al., 2005
		Malanshan	KK06032	K-rich rhyolite	Kfs Ar-Ar	8.91	0.18	Jiang et al., 2008
		Luangou Shan	KY7-15	Trachyandesite	WR K-Ar	17.04	0.34	Zheng and Bian, 1996
		Bukadaban	8306-1	K-rich rhyolite	WR K-Ar	8.86	1.20	Zhao et al., 2009
7	Wuxuefeng area	Wuxuefeng	KY8-22	Trachyandesite	WR K-Ar	21.24	0.28	Zheng and Bian, 1996
		Wuxuefeng	KK06022	Trachyte	WR K-Ar	17.82	0.34	Jiang et al., 2008
		Wuxuefeng	KK06024	Trachyte	WR K-Ar	12.74	0.28	Jiang et al., 2008
		Kebei lake	KY9-1	Trachyandesite	WR K-Ar	24.55	0.37	Zheng and Bian, 1996

Table DR1 (*continued*)

No.	Area	Locality	Sample No.	Lithology	Dating method	Age (Ma)	± 2σ	Data source
8	Kekao lake area	Kekao lake	HX1-11	Latite	WR K-Ar	11.70	0.30	Deng et al., 1996
		Kekao lake	HX1-15	Latite	WR K-Ar	14.47	0.22	Deng et al., 1996
		Kekao lake	HX2-1a	K-rich rhyolite	WR K-Ar	13.20	0.46	Deng et al., 1996
		Kekao lake	HX2-1b	K-rich rhyolite	WR K-Ar	11.70	0.30	Deng et al., 1996
		Kekao lake	KK06010	Trachyandesite	WR K-Ar	11.49	0.30	Jiang et al., 2008
		Kekao lake	KK06011	Trachyandesite	WR K-Ar	7.89	0.18	Jiang et al., 2008
		Dakanding	KP_{18}-17-1	Trachyandesite	Zr U-Pb	13.20	0.60	Wei et al., 2007
		Zhuonai lake	KY9-4	Quartz porphyry	WR K-Ar	11.93	0.19	Zheng and Bian, 1996
9	Damao Shan	Damao Shan	HX7-4	Trachyte	WR K-Ar	17.30	0.40	Deng et al., 1996
		Damao Shan	HX7-7	Trachydacite	WR K-Ar	15.39	0.30	Deng et al., 1996
		Damao Shan	KP_{21}-4-4	Trachydacite	Zr U-Pb	18.30	1.10	Wei et al., 2007
		Damao Shan	302	Trachyte	Zr U-Pb	17.67	0.38	Zhao et al., 2009
10	West Qinling	Daheba	DHB92-12	Shoshonite	WR Ar-Ar	11.10		Yu et al., 2011
		Guanjie	GJZ92-13	Shoshonite	WR Ar-Ar	10.80		Yu et al., 2011
		Maquangou	MJG0402	Shoshonite	WR Ar-Ar	9.63		Yu et al., 2011
		Haoti	HT-0309	Kamafugite	Phl Ar-Ar	17.82	0.44	Yu et al., 2006
		Haoti	HT92-1	Kamafugitic agglomerate	WR K-Ar	7.10		Yu et al., 1994
		Haoti	HT92-2	Kamafugite	WR K-Ar	7.90		Yu et al., 1994
		Haoti	HT92-3	Kamafugite	WR K-Ar	18.90		Yu et al., 1994
		Fenshuiling	FSL92-4	Kamafugite	WR K-Ar	18.30		Yu et al., 1994
		Wangping	WP92-5	Kamafugitic breccia	WR K-Ar	8.70		Yu et al., 1994
		Wangping	WP92-6	Kamafugite	WR K-Ar	13.80		Yu et al., 1994
		Niuding Shan	NDS92-7	Kamafugite	WR K-Ar	8.40		Yu et al., 1994
		Niuding Shan	ND02-01	Kamafugitic tuff	WR K-Ar	11.70		Yu et al., 2011
		Niuding Shan	ND02-02	Kamafugitic tuff	WR K-Ar	13.60		Yu et al., 2011
		Xiaoding Shan	XD-1	Kamafugite	Phl Ar-Ar	23.17		Yu et al., 2006
		Xiaoding Shan	XD-2	Kamafugite	Phl Ar-Ar	22.64		Yu et al., 2006
		Xiaoding Shan	XDS-8	Kamafugite	WR K-Ar	15.10		Yu et al., 2011
		Xiaoding Shan	XDS-9	Kamafugitic breccia	WR K-Ar	18.30		Yu et al., 2011
		Xiaoding Shan	XDS01-01	Kamafugitic agglomerate	WR K-Ar	15.70		Yu et al., 2011
		Shangwenjia	SWJ92-10	Kamafugitic agglomerate	WR K-Ar	13.10		Yu et al., 1994
		Shangwenjia	SWJ92-11	Kamafugite	WR K-Ar	14.60		Yu et al., 1994
		Shangdujia	LSS0302	Kamafugite	Phl Ar-Ar	23.09	0.30	Yu et al., 2006
		Shangdujia	STJ01-02	Kamafugitic agglomerate	WR K-Ar	14.70		Yu et al., 2011
		Shangdujia	STJ01-03	Kamafugite	WR K-Ar	14.90		Yu et al., 2011
		Baicao Shan	BCS01-04	Kamafugite	WR K-Ar	19.10		Yu et al., 2011
		Yinggeping	YGP01-05	Kamafugite	WR K-Ar	15.90		Yu et al., 2011
		Longwang Shan	CZ0303	Kamafugite	Phl Ar-Ar	22.31	0.36	Yu et al., 2006
		Longwang Shan	ZJ-0304	Kamafugite	Phl Ar-Ar	22.80	0.22	Yu et al., 2006
		Lixian	LX1506	Kamafugite	Prv U-Pb	16.58	0.46	This study
		Lixian	LX1608	Kamafugite	Prv U-Pb	20.35	0.89	This study
		Lixian	LX1511	Kamafugite	Prv U-Pb	19.92	0.80	This study
		Lixian	LX1525	Kamafugite	Prv U-Pb	16.19	0.42	This study

- Ap = apatite, Kfs = K-feldspar, Phl = phlogopite, Pl = plagioclase, Prv = perovskite, Sa = sanidine, WR = whole rock, Zr = zircon
- FT = fission track

Table DR2 **Major and trace element data of kamafugite samples, standards, and procedural blank**

	Kamafugite samples				International rock standards and procedural blank								
	LX1506	**LX1508**	**LX1511**	**LX1525**	**AGV-2**	**Ref.**	**BHVO-2**	**Ref.**	**BCR-2**	**Ref.**	**RGM-2**	**Ref.**	**Blank***
Major element (wt.%)													
SiO_2	40.7	39.8	39.5	39.3									
TiO_2	3.04	3.14	3.12	2.80									
Al_2O_3	9.58	7.67	7.65	8.91									
TFe_2O_3	11.35	11.37	11.17	10.92									
MnO	0.16	0.15	0.16	0.15									
MgO	12.68	15.72	18.49	15.05									
CaO	14.23	13.09	12.56	13.05									
Na_2O	1.61	1.80	0.96	1.53									
K_2O	1.06	1.12	0.64	1.09									
P_2O_5	1.11	1.63	1.48	1.19									
LOI	4.54	3.64	3.93	6.07									
Total	100.1	99.1	99.7	100.1									
K_2O/Na_2O	0.66	0.62	0.66	0.71									
$Mg^{\#}$	68.9	73.3	76.6	73.2									
Trace element (ppm)													
Li	31.1	11.2	7.11	12.5	9.74	11.0	3.99	4.80	8.24	9.00	60.4	57.0	0.0180
Be	2.00	2.14	2.19	1.73	2.07	2.30	1.09	1.00	2.00		2.55	2.37	0.0015
Sc	19.9	17.5	17.5	18.8	11.8	13.0	32.4	32.0	33.9	33.0	4.45	4.40	0.0030
V	193	159	158	174	118	120	319	317	417	416	12.0	13.0	0.2198
Cr	346	682	619	434	13.8	16.0	285	280	13.6	16.5	7.89	5.90	0.0448
Co	53.3	60.5	59.7	52.2	14.3	16.0	46.0	45.0	38.0	37.0	1.85	2.00	0.0068
Ni	326	512	509	376	17.3	20.0	124	119	11.3	13.0	5.46	5.20	0.0230
Cu	66.4	76.4	73.4	59.9	52.2	53.0	130	127	16.9	18.4	9.17	9.60	0.0209
Zn	111	115	109	102	87.1	86.0	103	103	131	133	33.2	32.0	0.0835
Ga	16.8	15.5	14.9	15.5	21.0	20.0	21.5	21.7	22.2	23.0	16.6	16.5	0.0038
Rb	22.3	32.3	16.6	24.4	67.8	66.3	8.5	9.1	46.3	46.9	150	150	0.0142
Sr	1209	1385	1622	1167	660	661	397	396	339	340	109	108	0.0524
Zr	318	383	386	301	230	230	167	172	183	184	226	220	0.0278
Nb	123	142	139	114	13.9	14.5	19.4	18.1	12.3	12.6	8.99	9.30	0.0022
Cs	1.33	0.35	0.26	0.18	1.12	1.16	0.10	0.10	1.10	1.10	9.64	9.60	0.0009
Ba	2936	619	1068	1117	1120	1130	130	131	665	677	835	810	0.1534
Hf	6.67	7.88	7.84	6.54	5.24	5.00	4.38	4.36	4.92	4.90	5.94	6.20	0.0008
Ta	5.32	5.81	5.50	5.24	0.87	0.87	1.15	1.14	0.80	0.78	0.92	0.95	0.0159
Pb	4.97	5.04	5.57	4.54	13.5	13.2	1.50	1.60	10.4	11.0	19.7	19.3	0.0116
Th	10.7	16.0	15.1	11.1	5.91	6.10	1.15	1.22	5.65	5.70	15.4	15.1	0.0010
U	1.83	3.28	3.07	2.58	1.94	1.86	0.42	0.40	1.71	1.69	5.68	5.80	0.0003
La	89.0	121	113	90.4	38.2	37.9	15.4	15.2	25.1	24.9	23.4	24.0	0.0035
Ce	170	233	217	167	69.5	68.6	37.2	37.5	53.0	52.9	46.3	47.0	0.0120
Pr	20.6	28.4	26.6	20.4	8.14	7.84	5.25	5.35	6.67	6.70	5.20	5.36	0.0008
Nd	79.5	108	102	79.2	30.6	30.5	24.4	24.5	28.5	28.7	19.2	19.0	0.0045
Sm	13.4	17.4	16.4	13.1	5.64	5.49	6.07	6.07	6.63	6.58	4.11	4.30	0.0007
Eu	4.00	5.17	4.95	3.95	1.56	1.54	2.09	2.07	1.97	1.96	0.61	0.66	0.0004
Gd	10.9	13.8	13.1	10.5	4.71	4.52	6.08	6.24	6.75	6.75	3.69	3.70	0.0010
Tb	1.35	1.65	1.57	1.35	0.66	0.64	0.95	0.92	1.07	1.07	0.61	0.66	0.0002
Dy	6.60	7.87	7.51	6.50	3.63	3.47	5.39	5.31	6.54	6.41	3.78	4.10	0.0007
Ho	1.06	1.18	1.13	0.99	0.67	0.65	0.99	0.98	1.30	1.28	0.77	0.82	0.0003
Er	2.43	2.59	2.50	2.23	1.86	1.81	2.50	2.54	3.71	3.66	2.29	2.35	0.0003
Tm	0.30	0.32	0.30	0.28	0.26	0.26	0.34	0.33	0.53	0.54	0.37	0.37	0.0000
Yb	1.60	1.65	1.62	1.59	1.69	1.62	1.97	2.00	3.43	3.38	2.51	2.60	0.0003
Lu	0.23	0.21	0.20	0.21	0.25	0.25	0.28	0.27	0.51	0.50	0.38	0.40	0.0001
Y	29.4	32.5	31.4	27.3	20.2	20.0	26.4	26.0	36.0	37.0	23.6	23.2	0.0036

- * Units are ppb for procedural blank.
- Recommended trace element compositions of international rock standards are from http://georem.mpch-mainz.gwdg.de/, http://minerals.cr.usgs.gov/geo_chem_stand/, and Govindaraju G. (1994).

Table DR3 **Major and trace element data of perovskites from west Qinling kamafugites**

	Perovskite sample LX1506											
	1	**2**	**3**	**4**	**5**	**6**	**7**	**8**	**9**	**10**	**11**	**12**
Major element (wt.%)												
SiO_2	0.17	0.06	0.14	0.03	0.05	0.09	0.06	0.09	0.03	0.05	0.08	0.10
TiO_2	54.8	55.5	54.9	55.7	55.8	55.5	55.7	55.7	55.6	54.4	55.4	54.3
Al_2O_3	0.20	0.19	0.18	0.17	0.21	0.20	0.12	0.15	0.14	0.12	0.18	0.06
FeO	0.93	1.04	1.02	0.80	0.84	0.76	0.77	0.77	0.75	0.81	0.88	0.78
MnO				0.01	0.02		0.04	0.02			0.04	0.05
MgO	0.03	0.06	0.04	0.02	0.00	0.03	0.03	0.01	0.02	0.01	0.01	0.05
CaO	38.1	38.2	38.5	38.0	37.8	38.3	37.8	38.3	38.3	37.7	38.2	37.4
Na_2O	0.37	0.36	0.45	0.52	0.47	0.45	0.59	0.59	0.49	0.55	0.49	0.60
K_2O	0.01	0.01	0.01	0.02		0.03		0.01	0.001	0.001	0.03	0.01
C_2O_3		0.01	0.02	0.03	0.01	0.01	0.06	0.08		0.01	0.001	
NiO	0.05		0.06	0.04	0.02				0.09		0.01	
Total	94.7	95.4	95.3	95.3	95.2	95.5	95.2	95.8	95.5	93.6	95.2	93.3
Trace element (ppm)												
Rb	4.67	0.81		1.36	3.24	0.13	0.43	6.23	2.64	1.55	0.46	
Sr	6566	3890		3233	3132	4583	3201	3587	2855	3237	5625	
Zr	164	146		175	159	179	154	165	172	153	182	
Nb	4745	4072		2504	3136	4163	2779	3346	2520	3239	5461	
Ba	138	35.8		78.5	84.0	20.2	44.8	73.6	77.5	81.4	30.3	
Hf	3.71	3.72		4.42	3.78	4.38	4.03	4.13	4.84	3.83	4.36	
Ta	273	332		239	282	249	295	329	260	291	427	
Pb	7.14	4.96		4.15	5.54	6.21	5.77	4.57	5.96	4.47	7.73	
Th	705	1207		1197	1126	584	1462	1429	1330	1157	1192	
U	158	128		67	84	157	70	86	65	89	179	
La	5679	5522		4697	5272	4288	5487	6001	5034	5459	6640	
Ce	10861	12563		11847	11513	7293	12651	13278	12269	11979	12489	
Pr	1039	1267		1241	1250	712	1412	1431	1339	1309	1249	
Nd	3728	4791		4795	4917	2655	5596	5540	5228	5089	4640	
Sm	591	695		644	718	480	763	769	708	725	718	
Eu	191	189		165	188	151	187	191	176	189	194	
Gd	338	356		298	358	321	369	378	333	369	404	
Tb	40.1	38.4		30.2	37.7	40.8	37.6	39.0	33.7	39.4	45.8	
Dy	166	150		112	146	178	142	148	126	150	191	
Ho	22.4	19.6		14.0	18.6	25.1	17.7	19.0	15.6	19.5	25.2	
Er	38.2	32.4		22.9	30.2	44.3	28.5	30.3	25.5	31.7	43.0	
Tm	3.34	2.73		1.91	2.47	3.97	2.31	2.48	2.13	2.71	3.62	
Yb	15.2	12.1		8.32	11.2	17.0	10.0	10.6	9.15	11.3	15.7	
Lu	1.16	0.99		0.70	0.91	1.46	0.84	0.90	0.65	1.01	1.28	
Y	392	326		239	319	456	298	319	263	331	432	
Rb/Sr	0.0007	0.0002		0.0004	0.0010	0.0000	0.0001	0.0017	0.0009	0.0005	0.0001	
Er/Sr	0.0058	0.0083		0.0071	0.0096	0.0097	0.0089	0.0085	0.0089	0.0098	0.0076	
Yb/Sr	0.0023	0.0031		0.0026	0.0036	0.0037	0.0031	0.0029	0.0032	0.0035	0.0028	
Sm/Nd	0.16	0.15		0.13	0.15	0.18	0.14	0.14	0.14	0.14	0.15	

Table DR3 (***continued***)

	Perovskite sample LX1508											
	1	**2**	**3**	**4**	**5**	**6**	**7**	**8**	**9**	**10**	**11**	**12**
Major element (wt.%)												
SiO_2	0.17	0.06	0.14	0.03	0.05	0.09	0.06	0.09	0.03	0.05	0.08	0.10
TiO_2	54.8	55.5	54.9	55.7	55.8	55.5	55.7	55.7	55.6	54.4	55.4	54.3
Al_2O_3	0.06	0.07	0.07	0.13	0.14	0.09	0.18	0.13	0.07	0.06	0.08	0.08
FeO	0.70	0.79	0.71	0.75	0.70	0.72	0.79	0.80	0.77	0.73	0.65	0.61
MnO			0.03	0.002	0.02		0.01			0.03	0.02	0.01
MgO	0.05	0.01	0.01	0.02	0.03	0.04	0.08	0.04	0.04	0.08	0.02	0.001
CaO	39.5	39.8	39.6	39.5	39.4	39.3	38.9	39.2	38.5	38.9	39.2	38.8
Na_2O	0.31	0.25	0.24	0.28	0.24	0.21	0.28	0.32	0.28	0.39	0.35	0.36
K_2O	0.03		0.01		0.01	0.02		0.01		0.03		0.01
C_2O_3	0.03	0.03	0.05	0.08	0.20	0.06	0.12	0.17	0.10	0.04	0.03	0.05
NiO	0.04	0.02	0.04	0.03	0.07			0.02	0.01	0.003		
Total	95.7	96.5	95.9	96.4	96.6	96.1	96.1	96.5	95.5	94.6	95.8	94.4
Trace element (ppm)												
Rb	0.54		1.09	1.51	0.42	0.64	0.60	0.28		< 0.121	0.33	0.34
Sr	3651		3015	3154	3179	3897	2878	2992		3349	2882	3000
Zr	383		260	257	241	353	178	234		311	194	259
Nb	3046		2056	2501	2482	3338	2227	2508		2950	2288	2403
Ba	50.2		130.8	148.7	47.9	50.5	83.1	41.1		23.7	29.5	59.7
Hf	9.45		7.90	7.31	7.16	8.75	5.69	7.19		8.53	6.27	7.75
Ta	71.7		155	151	122	66.4	169	172		88.6	185	133
Pb	9.62		3.63	3.99	4.52	5.39	3.41	3.56		4.10	3.59	3.54
Th	17.2		690	520	281	10.3	793	718		42.3	916	345
U	109		50.8	73.6	79.6	120	60.4	68.9		103	59.1	77.4
La	1919		3903	3782	3212	1679	4419	4261		2293	4632	3495
Ce	2035		8446	7369	5785	1891	10383	8716		3048	10446	6582
Pr	193		948	801	592	162	1111	977		281	1154	684
Nd	750		3815	3225	2334	594	4374	3976		1057	4598	2687
Sm	207		573	541	422	165	646	627		256	676	473
Eu	82.0		152	151	130	73.2	171	167		96.3	175	139
Gd	227		296	317	279	188	317	339		237	338	298
Tb	35.5		31.2	36.2	33.5	29.6	32.7	36.6		33.2	34.8	34.9
Dy	182		119	147	138	152	123	144		157	132	144
Ho	28.6		14.9	19.3	18.4	23.7	15.2	18.5		23.3	16.2	19.5
Er	53.6		24.8	32.4	31.4	45.4	23.5	30.3		41.7	25.8	32.3
Tm	5.19		2.06	2.89	2.69	4.38	1.97	2.66		3.73	2.12	2.93
Yb	24.9		9.46	13.3	13.2	20.7	8.76	12.1		17.4	9.59	12.5
Lu	2.17		0.78	1.15	1.08	1.81	0.72	0.98		1.55	0.72	1.11
Y	592		270	362	352	496	261	338		458	285	359
Rb/Sr	0.0001		0.0004	0.0005	0.0001	0.0002	0.0002	0.0001			0.0001	0.0001
Er/Sr	0.0147		0.0082	0.0103	0.0099	0.0116	0.0082	0.0101		0.0125	0.0089	0.0108
Yb/Sr	0.0068		0.0031	0.0042	0.0041	0.0053	0.0030	0.0040		0.0052	0.0033	0.0042
Sm/Nd	0.28		0.15	0.17	0.18	0.28	0.15	0.16		0.24	0.15	0.18

Table DR3 (***continued***)

	Perovskite sample LX1511											
	1	**2**	**3**	**4**	**5**	**6**	**7**	**8**	**9**	**10**	**11**	**12**
Major element (wt.%)												
SiO_2	0.04	0.06	0.04	0.04	0.03	0.02	0.06	0.03	0.03	0.05	0.02	0.04
TiO_2	56.4	56.9	56.6	56.2	57.3	57.0	56.3	56.9	56.3	56.6	56.9	56.8
Al_2O_3	0.02			0.10	0.06	0.06	0.07	0.09		0.01	0.06	0.06
FeO	0.59	0.53	0.54	0.71	0.67	0.63	0.59	0.50	0.49	0.49	0.57	0.66
MnO	0.04	0.02	0.03		0.05	0.02	0.04	0.05	0.03	0.04	0.01	
MgO		0.01	0.03	0.04		0.04		0.004	0.02	0.02	0.02	0.03
CaO	38.7	40.3	39.4	39.6	40.3	40.3	39.7	39.7	39.2	39.2	39.7	39.7
Na_2O	0.70	0.45	0.63	0.32	0.29	0.33	0.45	0.47	0.52	0.48	0.49	0.46
K_2O	0.01	0.01		0.01				0.01	0.01	0.01	0.02	
C_2O_3	0.06	0.02		0.06	0.04	0.03	0.03	0.07	0.002	0.07	0.03	0.06
NiO			0.05			0.05		0.06		0.02	0.01	0.03
Total	96.5	98.3	97.3	97.1	98.7	98.4	97.2	97.8	96.6	97.0	97.8	97.8
Trace element (ppm)												
Rb		< 0.110	< 0.117	< 0.132		0.15	0.21	< 0.150	0.25	0.17	< 0.100	0.24
Sr		4753	4879	3972		4745	4096	4954	5000	5043	4545	4533
Zr		326	328	337		380	387	378	365	372	333	379
Nb		3701	3745	3397		3692	3410	3775	3511	3848	3644	3631
Ba		41.4	43.7	31.8		41.0	31.7	67.2	276.3	44.3	35.8	37.3
Hf		8.32	8.15	8.43		9.76	10.16	9.55	9.06	9.07	8.07	9.75
Ta		62.4	61.4	70.2		65.0	63.9	67.5	65.2	67.0	69.6	65.1
Pb		6.38	6.40	5.72		7.46	6.66	7.55	7.72	6.15	5.04	15.03
Th		18.5	18.5	19.2		16.0	11.8	22.1	14.7	19.5	23.1	16.9
U		118	124	117		112	113	120	114	123	129	110
La		1778	1690	1901		1719	1670	1755	1626	1748	1741	1776
Ce		2202	2045	2289		1929	1827	1983	1757	1983	2081	2020
Pr		190	175	200		172	160	179	154	176	181	181
Nd		677	631	734		635	595	661	560	652	653	671
Sm		162	153	188		159	161	165	146	162	169	165
Eu		69.3	67.5	79.1		67.2	69.6	68.0	63.7	69.4	72.7	69.3
Gd		161	160	197		175	185	182	171	179	183	180
Tb		24.9	24.9	29.7		27.4	29.5	28.6	27.0	28.1	28.5	27.9
Dy		129	130	151		144	155	150	141	147	148	145
Ho		20.3	20.4	23.0		22.9	24.7	24.1	22.7	23.5	23.1	23.2
Er		38.7	39.7	43.4		44.5	47.6	46.5	43.9	45.3	45.0	44.6
Tm		3.77	3.87	4.15		4.31	4.63	4.54	4.35	4.40	4.30	4.28
Yb		17.6	18.3	19.4		20.1	21.1	20.8	20.2	21.0	20.3	20.0
Lu		1.49	1.54	1.70		1.71	1.83	1.83	1.71	1.75	1.75	1.68
Y		415	425	476		480	518	506	480	489	480	484
Rb/Sr						0.0000	0.0001		0.0000	0.0000		0.0001
Er/Sr		0.0081	0.0081	0.0109		0.0094	0.0116	0.0094	0.0088	0.0090	0.0099	0.0098
Yb/Sr		0.0037	0.0037	0.0049		0.0042	0.0052	0.0042	0.0040	0.0042	0.0045	0.0044
Sm/Nd		0.24	0.24	0.26		0.25	0.27	0.25	0.26	0.25	0.26	0.25

Table DR3 (***continued***)

	Perovskite sample LX1525											
	1	**2**	**3**	**4**	**5**	**6**	**7**	**8**	**9**	**10**	**11**	**12**
Major element (wt.%)												
SiO_2	0.08	0.03	0.05	0.03			0.05	0.05	0.02	0.03	0.02	
TiO_2	55.8	56.4	54.8	56.5	56.7	55.6	55.6	56.0	56.2	55.6	56.4	55.7
Al_2O_3	0.01	0.08		0.07	0.06			0.08				
FeO	0.65	0.73	0.52	0.68	0.52	0.32	0.64	0.52	0.39	0.36	0.56	0.34
MnO	0.03		0.05	0.03		0.02	0.06	0.05			0.01	0.02
MgO	0.02	0.04	0.04			0.02	0.02	0.01	0.05	0.02		0.02
CaO	37.5	38.3	36.4	37.9	37.9	35.8	37.0	37.2	37.0	36.3	37.1	37.0
Na_2O	0.87	0.66	0.98	0.82	0.79	1.35	1.02	1.00	1.27	1.20	1.00	1.20
K_2O	0.01	0.01		0.02		0.03		0.03	0.01	0.02	0.01	0.01
C_2O_3	0.01	0.002	0.02	0.01		0.05	0.02	0.01		0.01	0.02	
NiO	0.01		0.06	0.03	0.01		0.05	0.03	0.02	0.03	0.04	0.03
Total	95.0	96.3	93.0	96.1	95.9	93.2	94.5	94.9	95.0	93.6	95.1	94.3
Trace element (ppm)												
Rb	0.29		< 0.115	0.11	0.39		0.18	1.42	0.54	1.49	0.26	0.21
Sr	3107		3160	4277	3967		2955	6821	9443	4342	10534	10667
Zr	152		152	167	199		151	171	201	187	193	187
Nb	3136		3340	4507	3951		3044	5726	8338	4638	9158	9617
Ba	16.8		33.6	44.1	28.8		14.2	47.1	79.8	24.1	56.9	54.4
Hf	4.40		4.21	4.59	5.28		4.39	4.42	4.38	4.69	4.00	3.95
Ta	237.1		225.4	279.3	267.1		222.9	276.5	381.1	295.7	410.6	443.5
Pb	4.60		5.20	7.34	4.93		3.85	14.70	9.39	5.18	12.23	9.95
Th	860		678	707	816		747	592	593	771	608	703
U	89		104	149	127		89	177	289	153	303	333
La	4788		4666	5149	4876		4692	4613	5457	5095	6035	6188
Ce	10327		9749	9736	9763		9794	8239	8371	9583	8884	9020
Pr	1090		977	964	1000		1027	813	741	956	783	807
Nd	4243		3688	3616	3811		3993	3073	2616	3640	2725	2852
Sm	633		581	596	595		611	517	476	593	492	517
Eu	171		168	173	165		168	157	158	170	164	169
Gd	344		332	358	336		344	327	334	363	349	372
Tb	36.7		36.9	42.0	38.2		37.3	40.1	44.9	43.0	46.3	49.9
Dy	145		147	173	154		147	170	204	178	209	223
Ho	18.7		19.2	23.3	20.6		19.0	23.2	29.1	23.8	29.6	31.5
Er	30.8		32.1	38.4	33.8		31.1	39.9	51.3	40.2	51.4	54.9
Tm	2.57		2.72	3.29	2.84		2.71	3.42	4.60	3.53	4.58	4.75
Yb	11.1		12.9	14.3	13.1		11.6	14.8	19.5	15.0	18.8	20.0
Lu	0.94		1.00	1.09	1.09		1.03	1.21	1.50	1.22	1.45	1.54
Y	323		336	403	354		329	407	507	418	512	545
Rb/Sr	0.0001			0.0000	0.0001		0.0001	0.0002	0.0001	0.0003	0.0000	0.0000
Er/Sr	0.0099		0.0101	0.0090	0.0085		0.0105	0.0058	0.0054	0.0093	0.0049	0.0051
Yb/Sr	0.0036		0.0041	0.0033	0.0033		0.0039	0.0022	0.0021	0.0035	0.0018	0.0019
Sm/Nd	0.15		0.16	0.16	0.16		0.15	0.17	0.18	0.16	0.18	0.18

Table DR4 U-Pb age data of AFK standard and perovskites from the west Qinling kamafugites

Analysis spot	U (ppm)	Th (ppm)	Th/U	Isotopic ratios uncorrected				^{207}Pb correction	
				$^{207}Pb/^{206}Pb$	± 1σ (%)	$^{206}Pb/^{238}U$	± 1σ (%)	Age (Ma)	± 1σ (Ma)
AFK Standard									
AFK@1	142	1387	9.8	14.5715	1.8846	0.1644	0.4310	369.1	7.2
AFK@2	145	1180	8.2	15.1509	1.8936	0.1359	1.6107	370.1	8.0
AFK@3	132	1104	8.3	13.8310	1.8233	0.1654	0.6796	387.9	7.6
AFK@4	141	693	4.9	14.9193	1.9548	0.1257	0.6589	381.1	7.8
AFK@5	133	515	3.9	15.1891	1.9633	0.1280	0.9820	373.2	7.9
AFK@6	141	1295	9.2	14.1442	1.7915	0.1690	0.8351	377.5	7.4
AFK@7	143	1295	9.0	14.4083	1.8760	0.1639	0.6594	373.5	7.5
AFK@8	129	1346	10.4	13.6602	1.8097	0.1719	0.7419	389.0	7.6
AFK@9	121	1062	8.8	14.4079	1.8136	0.1587	1.0902	376.3	7.7
AFK@10	137	1154	8.4	13.9523	1.5555	0.1696	0.8846	382.2	6.7
AFK@11	139	1193	8.6	13.9777	1.5170	0.1546	0.4388	390.0	6.2
AFK@12	142	499	3.5	15.4899	1.3241	0.1242	0.7626	368.0	5.3
AFK@13	135	1142	8.5	13.9097	1.3629	0.1713	0.3557	382.5	5.5
AFK@14	138	1112	8.1	14.0626	1.4218	0.1609	0.5998	384.2	5.9
AFK@15	143	1007	7.1	14.2015	1.4144	0.1603	0.6419	380.8	5.9
AFK@16	93	1177	12.6	12.4950	1.7548	0.2517	0.8995	374.4	7.9
AFK@17	137	1143	8.4	15.0446	1.4172	0.1193	1.3659	381.3	6.2
Sample LX1506									
LX1506@1	46	1082	23.3	0.6460	2.7387	82.7139	2.8125	18.7	2.3
LX1506@2	50	627	12.6	0.6690	3.6693	89.5785	3.9902	15.2	2.8
LX1506@3	77	759	9.8	0.6420	0.8110	92.9312	1.4028	17.0	0.7
LX1506@4	60	856	14.3	0.6281	2.5565	93.9917	2.2709	18.0	1.8
LX1506@5	80	770	9.6	0.6474	1.2679	94.6889	1.6373	16.2	1.0
LX1506@6	68	893	13.1	0.6153	2.8740	92.2548	2.0996	19.5	2.0
LX1506@7	89	502	5.6	0.6624	1.8367	79.6460	1.4164	17.7	1.5
LX1506@8	72	981	13.6	0.6510	1.0217	94.5756	2.2236	15.9	0.9
LX1506@9	73	968	13.3	0.6251	2.2921	98.2253	1.8136	17.5	1.5
LX1506@10	81	916	11.3	0.6160	2.3953	100.6283	1.6143	17.8	1.5
LX1506@11	69	939	13.7	0.6689	1.2304	101.2924	1.7672	13.4	0.9
LX1506@12	131	737	5.6	0.5560	1.7225	138.1599	1.9008	16.5	0.9
LX1506@13	79	1011	12.8	0.6155	0.8519	97.6059	2.8399	18.4	1.0
LX1506@14	76	1010	13.3	0.6481	2.2485	104.7510	2.5291	14.6	1.5
LX1506@15	88	521	5.9	0.6583	1.6561	93.1790	1.6444	15.5	1.2
LX1506@16	82	833	10.1	0.6678	2.2638	86.4196	2.0149	15.8	1.7
LX1506@17	65	943	14.4	0.6188	1.7185	95.5332	1.8764	18.5	1.3
LX1506@18	102	629	6.1	0.6650	1.2412	92.6860	1.7851	15.0	1.0
LX1506@19	148	2480	16.8	0.6693	1.4185	76.3905	1.4641	17.8	1.3
LX1506@20	57	893	15.8	0.6679	3.0062	83.2653	2.7477	16.4	2.4
LX1506@21	60	815	13.6	0.6072	2.4096	95.9203	1.8848	19.4	1.6
LX1506@22	112	929	8.3	0.6690	1.8061	78.0177	2.2913	17.4	1.7
LX1506@23	84	647	7.7	0.6373	2.6284	93.3831	1.7684	17.3	1.8
LX1506@24	79	982	12.4	0.6150	2.3762	102.3769	2.0471	17.6	1.5
LX1506@25	79	1425	18.1	0.6648	1.9310	79.7178	1.7414	17.5	1.6
LX1506@26	69	924	13.4	0.6328	1.7700	97.4101	1.4703	17.0	1.2
LX1506@27	76	969	12.8	0.5858	2.1894	104.8584	3.0570	19.4	1.6
LX1506@28	270	1233	4.6	0.6127	1.0219	108.9829	1.2971	16.7	0.7
LX1506@29	179	759	4.3	0.6201	1.4082	100.0615	1.7913	17.6	1.0
LX1506@30	60	824	13.7	0.6583	2.9449	96.3432	2.5896	15.0	2.0
LX1506@31	106	596	5.6	0.6296	1.6555	101.4940	1.3992	16.6	1.1
LX1506@32	296	1492	5.0	0.6855	1.3929	76.1276	1.3584	16.1	1.2
LX1506@33	55	695	12.7	0.6709	2.6821	84.8010	2.3262	15.8	2.1
LX1506@34	239	605	2.5	0.6386	1.3689	103.7735	1.3766	15.5	0.9
LX1506@35	123	475	3.9	0.6772	1.1656	86.5243	1.4903	14.9	1.0
LX1506@36	44	1033	23.6	0.6704	2.8540	83.9961	2.4473	16.0	2.2

Table DR4 (*continued*)

Analysis spot	U (ppm)	Th (ppm)	Th/U	Isotopic ratios uncorrected				^{207}Pb correction	
				^{207}Pb/^{206}Pb	± 1σ (%)	^{206}Pb/^{238}U	± 1σ (%)	Age (Ma)	± 1σ (Ma)
Sample LX1508									
LX1508@1	50	59	1.2	0.6699	1.7388	80.7158	2.1365	16.8	1.5
LX1508@2	87	447	0.1	0.6775	1.3824	61.6489	1.3283	20.9	1.5
LX1508@3	37	233	11.2	0.6398	0.6513	79.4914	2.2748	20.1	0.9
LX1508@4	49	229	4.7	0.6220	2.1324	78.8138	2.0522	22.1	1.8
LX1508@5	45	65	2.0	0.6202	2.8878	74.5923	2.2151	23.5	2.5
LX1508@6	38	243	13.0	0.6960	3.1954	72.2816	1.9522	15.8	2.8
LX1508@7	58	384	1.0	0.6249	0.9972	79.4063	1.9410	21.6	1.1
LX1508@8	48	65	6.7	0.6335	1.3302	73.5818	2.3439	22.4	1.5
LX1508@9	42	31	7.9	0.6309	2.3621	72.4625	2.4097	23.0	2.2
LX1508@10	71	12	0.1	0.6750	2.1806	78.0190	1.8965	16.8	1.9
LX1508@11	50	417	4.0	0.6052	2.6004	83.6080	2.1651	22.5	2.0
LX1508@12	38	230	11.9	0.6398	3.3595	75.9887	2.7443	21.0	2.9
LX1508@13	89	89	0.3	0.6893	1.2497	55.9797	1.3681	21.3	1.5
LX1508@14	55	497	2.4	0.6168	2.2806	84.5189	3.2160	21.1	2.0
LX1508@15	66	56	0.1	0.6535	2.7091	79.3697	2.1659	18.7	2.2
LX1508@16	58	321	0.2	0.6615	2.0592	71.9218	2.8090	19.7	2.1
LX1508@17	61	335	0.4	0.6870	2.4139	82.0546	1.5832	14.8	1.9
LX1508@18	63	6	0.5	0.6216	2.0067	77.6112	1.3590	22.5	1.6
LX1508@19	41	201	11.6	0.6227	2.2319	76.6431	1.8455	22.7	1.9
LX1508@20	46	26	5.0	0.6237	1.4564	76.8556	1.9456	22.5	1.4
LX1508@21	48	132	4.9	0.6720	1.9574	82.7337	2.6141	16.1	1.7
LX1508@22	46	6	5.0	0.6494	2.9807	73.2557	2.7380	20.7	2.7
LX1508@23	60	14	1.1	0.6298	2.5306	77.0348	2.3156	21.8	2.2
LX1508@24	47	22	5.2	0.6335	2.5112	87.1806	1.8254	18.9	1.8
LX1508@25	46	30	8.3	0.6230	2.9674	84.5873	2.5988	20.5	2.3
LX1508@26	56	477	1.2	0.6370	3.0094	86.8797	2.1462	18.6	2.2
LX1508@27	63	228	0.5	0.6573	1.8812	75.6729	2.7256	19.2	1.9
Sample LX1511									
LX1511@1	76	13	0.2	0.7083	2.0252	57.5087	2.4879	18.1	2.5
LX1511@2	115	24	0.2	0.6814	1.2520	65.2051	1.8301	19.3	1.4
LX1511@3	68	45	0.7	0.6202	1.9404	84.7325	2.9959	20.7	1.8
LX1511@4	89	8	0.1	0.6868	1.7215	69.3738	2.0873	17.5	1.8
LX1511@5	70	3	0.0	0.6682	0.9736	61.9218	2.3556	22.0	1.4
LX1511@6	71	12	0.2	0.6200	1.0648	79.7021	2.2910	22.1	1.2
LX1511@7	81	13	0.2	0.7026	1.7049	58.5668	1.7760	18.5	2.0
LX1511@8	86	8	0.1	0.6844	2.0071	65.0925	2.1009	18.9	2.1
LX1511@9	90	14	0.2	0.6524	1.9803	71.4767	2.0110	20.9	1.9
LX1511@10	76	5	0.1	0.6981	1.7484	64.2809	1.9567	17.4	1.9
LX1511@11	91	14	0.2	0.6919	1.9394	63.2086	2.7759	18.5	2.2
LX1511@12	89	7	0.1	0.6987	1.8166	66.5141	2.1629	16.8	1.9
LX1511@13	103	18	0.2	0.6675	1.6150	80.0670	2.6351	17.1	1.5
LX1511@14	94	11	0.1	0.6616	0.9761	68.0044	2.0357	20.9	1.2
LX1511@15	127	34	0.3	0.6640	1.5803	71.4334	2.4098	19.6	1.7
LX1511@16	71	46	0.7	0.6221	1.1843	76.8118	2.3678	22.7	1.3
LX1511@17	103	15	0.1	0.6714	0.9690	69.4667	2.0527	19.3	1.2
LX1511@18	129	26	0.2	0.6785	1.5333	71.5003	2.3921	17.9	1.6
LX1511@19	73	11	0.2	0.6713	1.2474	56.9663	2.4206	23.5	1.8
LX1511@20	91	12	0.1	0.6687	1.5102	79.7217	3.1348	17.1	1.6
LX1511@21	90	12	0.1	0.6517	2.6064	72.0482	2.5151	20.8	2.4
LX1511@22	68	19	0.3	0.6473	2.2555	84.0840	3.0210	18.3	2.0
LX1511@23	100	21	0.2	0.6511	1.7102	84.7355	4.7200	17.8	1.9
LX1511@24	79	5	0.1	0.6620	3.1584	78.6064	3.0061	18.0	2.7
LX1511@25	66	5	0.1	0.6484	1.2045	69.3795	2.8258	22.0	1.5
LX1511@26	43	446	10.4	0.6265	2.0208	84.4642	3.6519	20.2	2.0

Table DR4 (***continued***)

Analysis spot	U (ppm)	Th (ppm)	Th/U	Isotopic ratios uncorrected				^{207}Pb correction	
				^{207}Pb/^{206}Pb	± 1σ (%)	^{206}Pb/^{238}U	± 1σ (%)	Age (Ma)	± 1σ (Ma)
Sample LX1525									
LX1525@1	61	598	9.8	0.6334	2.0416	101.3029	1.9279	16.3	1.4
LX1525@2	97	392	4.0	0.6152	1.6948	114.9030	2.3493	15.6	1.1
LX1525@3	283	642	2.3	0.5877	1.5637	121.4004	2.1154	16.7	1.0
LX1525@4	59	587	10.0	0.6625	2.4314	98.0981	2.5579	14.4	1.7
LX1525@5	58	544	9.4	0.6406	2.8740	95.2405	2.4999	16.7	2.0
LX1525@6	58	635	11.0	0.6275	2.3827	94.6353	3.1680	17.9	1.9
LX1525@7	167	303	1.8	0.6311	1.1005	108.8383	1.9658	15.3	0.8
LX1525@8	64	557	8.6	0.6130	2.2989	93.3412	2.6368	19.5	1.7
LX1525@9	212	331	1.6	0.6282	1.3274	102.4022	1.9835	16.5	1.0
LX1525@10	50	593	11.8	0.6867	1.8871	90.1095	2.4732	13.5	1.5
LX1525@11	159	323	2.0	0.6507	1.3857	95.5856	1.7997	15.8	1.1
LX1525@12	232	443	1.9	0.6416	1.1495	98.7730	1.9095	16.0	0.9
LX1525@13	90	488	5.4	0.6308	1.2595	107.1643	2.1231	15.6	0.9
LX1525@14	64	540	8.5	0.6622	1.9568	96.9185	2.1589	14.6	1.4
LX1525@15	50	670	13.4	0.6899	2.9857	73.2778	2.5407	16.2	2.7
LX1525@16	227	118	0.5	0.6527	1.6063	96.0409	2.2994	15.5	1.2
LX1525@17	145	462	3.2	0.5918	1.6705	109.7232	2.7252	18.1	1.2
LX1525@18	75	698	9.3	0.6267	1.9434	111.3252	2.0518	15.3	1.2
LX1525@19	324	448	1.4	0.6061	0.8627	117.1862	2.2197	16.0	0.7
LX1525@20	85	402	4.7	0.6729	2.6351	86.3093	3.1432	15.4	2.2
LX1525@21	52	568	10.9	0.6629	1.5749	91.5124	2.4667	15.4	1.3
LX1525@22	233	646	2.8	0.5921	1.5904	114.2602	2.1751	17.4	1.0
LX1525@23	49	609	12.3	0.6448	2.8650	81.1700	2.4631	19.2	2.3
LX1525@24	158	333	2.1	0.6380	2.3263	115.5466	2.4486	14.0	1.4
LX1525@25	107	408	3.8	0.6005	1.7814	99.5940	2.3053	19.3	1.3
LX1525@26	207	521	2.5	0.6169	1.1089	106.5284	2.4905	16.7	0.9
LX1525@27	239	537	2.2	0.6241	0.8101	104.6488	2.2016	16.5	0.8
LX1525@28	183	401	2.2	0.6522	2.6686	89.5473	2.5465	16.7	2.0
LX1525@29	197	454	2.3	0.6468	1.4366	93.2924	2.0398	16.5	1.1

Table DR5 Rb-Sr isotopic data of AFK standard and perovskites from the west Qinling kamafugites

Analysis spot	Age (Ma)	$^{84}Sr/^{86}Sr$	2σ	$^{84}Sr/^{88}Sr$	2σ	$^{87}Rb/^{86}Sr$	2σ	$^{87}Sr/^{86}Sr$	2σ	$^{87}Sr/^{86}Sr_i$	2σ
AFK Standard											
AFK@1	379	0.05737	0.00020	0.00685	0.00002	0.00007	0.00001	0.70316	0.00006	0.70316	0.00006
AFK@2	379	0.05682	0.00038	0.00678	0.00005	0.00008	0.00001	0.70306	0.00011	0.70306	0.00011
AFK@3	379	0.05764	0.00041	0.00688	0.00005	0.00016	0.00002	0.70349	0.00011	0.70349	0.00011
AFK@4	379	0.05777	0.00038	0.00690	0.00005	0.00011	0.00001	0.70331	0.00011	0.70331	0.00011
AFK@5	379	0.05834	0.00035	0.00697	0.00004	0.00017	0.00002	0.70372	0.00009	0.70372	0.00009
AFK@6	379	0.05727	0.00037	0.00684	0.00004	0.00016	0.00001	0.70342	0.00009	0.70342	0.00009
AFK@7	379	0.05752	0.00036	0.00687	0.00004	0.00009	0.00001	0.70335	0.00010	0.70335	0.00010
AFK@8	379	0.05735	0.00037	0.00685	0.00004	0.00009	0.00001	0.70336	0.00012	0.70336	0.00012
AFK@9	379	0.05710	0.00036	0.00682	0.00004	0.00008	0.00001	0.70345	0.00010	0.70345	0.00010
AFK@10	379	0.05728	0.00033	0.00684	0.00004	0.00008	0.00001	0.70339	0.00010	0.70339	0.00010
AFK@11	379	0.05746	0.00042	0.00686	0.00005	0.00010	0.00001	0.70322	0.00010	0.70322	0.00010
AFK@12	379	0.05743	0.00047	0.00686	0.00006	0.00015	0.00002	0.70346	0.00011	0.70346	0.00011
AFK@13	379	0.05693	0.00039	0.00680	0.00005	0.00009	0.00002	0.70335	0.00009	0.70335	0.00009
AFK@14	379	0.05629	0.00039	0.00672	0.00005	0.00009	0.00002	0.70332	0.00010	0.70332	0.00010
AFK@15	379	0.05730	0.00042	0.00684	0.00005	0.00014	0.00001	0.70344	0.00010	0.70344	0.00010
AFK@16	379	0.05677	0.00037	0.00678	0.00004	0.00010	0.00001	0.70329	0.00010	0.70328	0.00010
AFK@17	379	0.05755	0.00040	0.00687	0.00005	0.00014	0.00001	0.70330	0.00011	0.70330	0.00011
AFK@18	379	0.05709	0.00040	0.00682	0.00005	0.00010	0.00001	0.70337	0.00010	0.70337	0.00010
AFK@19	379	0.05754	0.00037	0.00687	0.00004	0.00014	0.00002	0.70321	0.00010	0.70321	0.00010
AFK@20	379	0.05714	0.00039	0.00682	0.00005	0.00010	0.00001	0.70330	0.00009	0.70330	0.00009
AFK@21	379	0.05703	0.00040	0.00681	0.00005	0.00011	0.00001	0.70330	0.00010	0.70330	0.00010
AFK@22	379	0.05736	0.00035	0.00685	0.00004	0.00017	0.00002	0.70335	0.00010	0.70335	0.00010
AFK@23	379	0.05700	0.00036	0.00681	0.00004	0.00009	0.00001	0.70333	0.00010	0.70333	0.00010
AFK@24	379	0.05677	0.00037	0.00678	0.00004	0.00009	0.00001	0.70344	0.00009	0.70344	0.00009
AFK@25	379	0.05722	0.00038	0.00683	0.00005	0.00010	0.00002	0.70330	0.00011	0.70330	0.00011
AFK@26	379	0.05708	0.00033	0.00682	0.00004	0.00008	0.00001	0.70324	0.00009	0.70324	0.00009
AFK@27	379	0.05713	0.00031	0.00682	0.00004	0.00006	0.00001	0.70326	0.00009	0.70326	0.00009
AFK@28	379	0.05661	0.00036	0.00676	0.00004	0.00009	0.00001	0.70341	0.00007	0.70341	0.00007
AFK@29	379	0.05652	0.00052	0.00675	0.00006	0.00012	0.00002	0.70336	0.00013	0.70336	0.00013
AFK@30	379	0.05626	0.00042	0.00672	0.00005	0.00010	0.00002	0.70344	0.00010	0.70344	0.00010
AFK@31	379	0.05673	0.00040	0.00677	0.00005	0.00010	0.00002	0.70330	0.00010	0.70330	0.00010
AFK@32	379	0.05615	0.00038	0.00670	0.00005	0.00007	0.00002	0.70325	0.00011	0.70325	0.00011
AFK@33	379	0.05644	0.00041	0.00674	0.00005	0.00007	0.00002	0.70325	0.00010	0.70325	0.00010
AFK@34	379	0.05675	0.00043	0.00678	0.00005	0.00009	0.00002	0.70343	0.00010	0.70343	0.00010
AFK@35	379	0.05686	0.00040	0.00679	0.00005	0.00008	0.00002	0.70324	0.00010	0.70324	0.00010
AFK@36	379	0.05658	0.00042	0.00676	0.00005	0.00010	0.00002	0.70334	0.00010	0.70334	0.00010
AFK@37	379	0.05692	0.00035	0.00680	0.00004	0.00008	0.00002	0.70336	0.00009	0.70336	0.00009
AFK@38	379	0.05668	0.00040	0.00677	0.00005	0.00010	0.00002	0.70333	0.00010	0.70333	0.00010
AFK@39	379	0.05719	0.00040	0.00683	0.00005	0.00008	0.00002	0.70344	0.00009	0.70344	0.00009
AFK@40	379	0.05685	0.00036	0.00679	0.00004	0.00011	0.00002	0.70336	0.00009	0.70336	0.00009
AFK@41	379	0.05640	0.00037	0.00673	0.00004	0.00006	0.00001	0.70332	0.00010	0.70332	0.00010
AFK@42	379	0.05688	0.00038	0.00679	0.00005	0.00007	0.00001	0.70333	0.00010	0.70333	0.00010
AFK@43	379	0.05673	0.00036	0.00677	0.00004	0.00008	0.00001	0.70332	0.00010	0.70332	0.00010
AFK@44	379	0.05622	0.00037	0.00671	0.00004	0.00006	0.00001	0.70336	0.00010	0.70336	0.00010
AFK@45	379	0.05649	0.00030	0.00675	0.00004	0.00010	0.00002	0.70334	0.00009	0.70334	0.00009
AFK@46	379	0.05708	0.00036	0.00682	0.00004	0.00006	0.00001	0.70342	0.00011	0.70342	0.00011
AFK@47	379	0.05663	0.00046	0.00676	0.00006	0.00006	0.00002	0.70333	0.00011	0.70333	0.00011
AFK@48	379	0.05669	0.00042	0.00677	0.00005	0.00009	0.00002	0.70337	0.00010	0.70337	0.00010
AFK@49	379	0.05696	0.00043	0.00680	0.00005	0.00005	0.00002	0.70343	0.00011	0.70343	0.00011
AFK@50	379	0.05654	0.00040	0.00675	0.00005	0.00003	0.00002	0.70338	0.00010	0.70338	0.00010
AFK@51	379	0.05659	0.00045	0.00676	0.00005	0.00006	0.00002	0.70342	0.00010	0.70342	0.00010
Sample LX1506											
LX1506@1	16.58	0.05739	0.00035	0.00685	0.00004	0.00039	0.00005	0.70431	0.00010	0.70431	0.00010
LX1506@2	16.58	0.05728	0.00029	0.00684	0.00003	0.00072	0.00007	0.70357	0.00008	0.70357	0.00008

Table DR5 (***continued***)

Analysis spot	Age (Ma)	$^{84}Sr/^{86}Sr$	2σ	$^{84}Sr/^{88}Sr$	2σ	$^{87}Rb/^{86}Sr$	2σ	$^{87}Sr/^{86}Sr$	2σ	$^{87}Sr/^{86}Sr_i$	2σ
LX1506@3	16.58	0.05712	0.00022	0.00682	0.00003	0.00080	0.00006	0.70331	0.00007	0.70331	0.00007
LX1506@4	16.58	0.05690	0.00030	0.00679	0.00004	0.00052	0.00016	0.70361	0.00009	0.70361	0.00009
LX1506@5	16.58	0.05706	0.00027	0.00681	0.00003	0.00009	0.00001	0.70322	0.00009	0.70322	0.00009
LX1506@6	16.58	0.05718	0.00033	0.00683	0.00004	0.00009	0.00002	0.70359	0.00009	0.70359	0.00009
LX1506@7	16.58	0.05744	0.00020	0.00686	0.00002	0.00014	0.00006	0.70319	0.00008	0.70319	0.00008
LX1506@8	16.58	0.05765	0.00028	0.00688	0.00003	0.00010	0.00001	0.70349	0.00008	0.70349	0.00008
LX1506@9	16.58	0.05733	0.00032	0.00684	0.00004	0.00010	0.00001	0.70370	0.00009	0.70370	0.00009
LX1506@10	16.58	0.05720	0.00031	0.00683	0.00004	0.00032	0.00001	0.70361	0.00008	0.70361	0.00008
LX1506@11	16.58	0.05705	0.00025	0.00681	0.00003	0.00120	0.00012	0.70327	0.00008	0.70327	0.00008
LX1506@12	16.58	0.05816	0.00051	0.00694	0.00006	0.00031	0.00002	0.70653	0.00012	0.70653	0.00012
LX1506@13	16.58	0.05732	0.00031	0.00684	0.00004	0.00018	0.00002	0.70371	0.00009	0.70371	0.00009
LX1506@14	16.58	0.05709	0.00033	0.00682	0.00004	0.00063	0.00012	0.70355	0.00009	0.70355	0.00009
LX1506@15	16.58	0.05734	0.00022	0.00685	0.00003	0.00011	0.00001	0.70330	0.00008	0.70330	0.00008
LX1506@16	16.58	0.05691	0.00017	0.00679	0.00002	0.00018	0.00004	0.70305	0.00006	0.70305	0.00006
LX1506@17	16.58	0.05763	0.00035	0.00688	0.00004	0.00012	0.00001	0.70374	0.00009	0.70374	0.00009
LX1506@18	16.58	0.05693	0.00026	0.00680	0.00003	0.00094	0.00011	0.70322	0.00008	0.70322	0.00008
LX1506@19	16.58	0.05678	0.00007	0.00678	0.00001	0.00006	0.00001	0.70260	0.00004	0.70260	0.00004
LX1506@20	16.58	0.05696	0.00028	0.00680	0.00003	0.00149	0.00004	0.70328	0.00008	0.70328	0.00008
LX1506@21	16.58	0.05702	0.00026	0.00681	0.00003	0.00039	0.00004	0.70348	0.00008	0.70348	0.00008
LX1506@22	16.58	0.05676	0.00008	0.00678	0.00001	0.00003	0.00000	0.70265	0.00005	0.70265	0.00005
LX1506@23	16.58	0.05749	0.00024	0.00686	0.00003	0.00013	0.00001	0.70345	0.00007	0.70345	0.00007
LX1506@24	16.58	0.05711	0.00031	0.00682	0.00004	0.00012	0.00001	0.70359	0.00008	0.70359	0.00008
LX1506@25	16.58	0.05676	0.00022	0.00678	0.00003	0.00036	0.00001	0.70319	0.00007	0.70319	0.00007
LX1506@26	16.58	0.05719	0.00034	0.00683	0.00004	0.00013	0.00001	0.70362	0.00009	0.70362	0.00009
LX1506@27	16.58	0.05758	0.00029	0.00687	0.00004	0.00121	0.00006	0.70369	0.00008	0.70369	0.00008
LX1506@28	16.58	0.05687	0.00007	0.00679	0.00001	0.00003	0.00000	0.70264	0.00004	0.70264	0.00004
LX1506@29	16.58	0.05728	0.00018	0.00684	0.00002	0.00012	0.00001	0.70329	0.00007	0.70329	0.00007
LX1506@30	16.58	0.05701	0.00013	0.00681	0.00002	0.00030	0.00003	0.70301	0.00005	0.70301	0.00005
LX1506@31	16.58	0.05744	0.00022	0.00686	0.00003	0.00013	0.00001	0.70336	0.00007	0.70336	0.00007
LX1506@32	16.58	0.05674	0.00004	0.00677	0.00001	0.00005	0.00000	0.70257	0.00003	0.70257	0.00003
LX1506@33	16.58	0.05772	0.00043	0.00689	0.00005	0.00126	0.00022	0.70385	0.00010	0.70385	0.00010
LX1506@34	16.58	0.05697	0.00007	0.00680	0.00001	0.00004	0.00000	0.70263	0.00004	0.70263	0.00004
LX1506@35	16.58	0.05717	0.00017	0.00683	0.00002	0.00010	0.00001	0.70315	0.00006	0.70315	0.00006
LX1506@36	16.58	0.05700	0.00029	0.00681	0.00004	0.00063	0.00005	0.70354	0.00008	0.70354	0.00008
Sample LX1508											
LX1508@1	20.35	0.05665	0.00036	0.00676	0.00004	0.00053	0.00004	0.70358	0.00008	0.70358	0.00008
LX1508@2	20.35	0.05704	0.00026	0.00681	0.00003	0.00104	0.00003	0.70330	0.00007	0.70330	0.00007
LX1508@3	20.35	0.05686	0.00045	0.00679	0.00005	0.00061	0.00003	0.70355	0.00012	0.70355	0.00012
LX1508@4	20.35	0.05696	0.00036	0.00680	0.00004	0.00013	0.00001	0.70369	0.00009	0.70369	0.00009
LX1508@5	20.35	0.05741	0.00034	0.00685	0.00004	0.00319	0.00017	0.70354	0.00008	0.70354	0.00008
LX1508@6	20.35	0.05721	0.00033	0.00683	0.00004	0.00060	0.00007	0.70366	0.00008	0.70366	0.00008
LX1508@7	20.35	0.05715	0.00031	0.00682	0.00004	0.00092	0.00003	0.70376	0.00008	0.70376	0.00008
LX1508@8	20.35	0.05766	0.00026	0.00688	0.00003	0.00028	0.00002	0.70361	0.00008	0.70361	0.00008
LX1508@9	20.35	0.05723	0.00036	0.00683	0.00004	0.00028	0.00004	0.70382	0.00009	0.70382	0.00009
LX1508@10	20.35	0.05729	0.00023	0.00684	0.00003	0.00013	0.00001	0.70331	0.00008	0.70331	0.00008
LX1508@11	20.35	0.05690	0.00025	0.00679	0.00003	0.00077	0.00006	0.70361	0.00008	0.70361	0.00008
LX1508@12	20.35	0.05730	0.00037	0.00684	0.00004	0.00114	0.00006	0.70378	0.00009	0.70378	0.00009
LX1508@13	20.35	0.05699	0.00013	0.00680	0.00002	0.00016	0.00001	0.70293	0.00005	0.70293	0.00005
LX1508@14	20.35	0.05751	0.00035	0.00687	0.00004	0.00051	0.00007	0.70361	0.00008	0.70361	0.00008
LX1508@15	20.35	0.05721	0.00028	0.00683	0.00003	0.00107	0.00014	0.70351	0.00007	0.70351	0.00007
LX1508@16	20.35	0.05728	0.00030	0.00684	0.00004	0.00096	0.00004	0.70368	0.00008	0.70368	0.00008
LX1508@17	20.35	0.05743	0.00036	0.00686	0.00004	0.00012	0.00002	0.70393	0.00008	0.70393	0.00008
LX1508@18	20.35	0.05724	0.00027	0.00683	0.00003	0.00023	0.00002	0.70353	0.00007	0.70353	0.00007
LX1508@19	20.35	0.05706	0.00041	0.00681	0.00005	0.00599	0.00056	0.70382	0.00010	0.70382	0.00010
LX1508@20	20.35	0.05697	0.00044	0.00680	0.00005	0.00037	0.00002	0.70391	0.00008	0.70391	0.00008

Table DR5 (***continued***)

Analysis spot	Age (Ma)	$^{84}Sr/^{86}Sr$	2σ	$^{84}Sr/^{88}Sr$	2σ	$^{87}Rb/^{86}Sr$	2σ	$^{87}Sr/^{86}Sr$	2σ	$^{87}Sr/^{86}Sr_i$	2σ
LX1508@21	20.35	0.05683	0.00034	0.00679	0.00004	0.00045	0.00004	0.70358	0.00008	0.70358	0.00008
LX1508@22	20.35	0.05725	0.00033	0.00684	0.00004	0.00068	0.00006	0.70383	0.00008	0.70383	0.00008
LX1508@23	20.35	0.05704	0.00024	0.00681	0.00003	0.00061	0.00008	0.70379	0.00006	0.70379	0.00006
LX1508@24	20.35	0.05762	0.00037	0.00688	0.00004	0.00030	0.00002	0.70378	0.00009	0.70378	0.00009
LX1508@25	20.35	0.05726	0.00035	0.00684	0.00004	0.00667	0.00062	0.70391	0.00009	0.70390	0.00009
LX1508@26	20.35	0.05720	0.00028	0.00683	0.00003	0.00015	0.00001	0.70369	0.00007	0.70369	0.00007
LX1508@27	20.35	0.05769	0.00032	0.00689	0.00004	0.00021	0.00001	0.70385	0.00007	0.70385	0.00007
Sample LX1511											
LX1511@1	19.92	0.05697	0.00015	0.00680	0.00002	0.00131	0.00025	0.70318	0.00006	0.70318	0.00006
LX1511@2	19.92	0.05719	0.00022	0.00683	0.00003	0.00011	0.00001	0.70350	0.00007	0.70350	0.00007
LX1511@3	19.92	0.05702	0.00024	0.00681	0.00003	0.00011	0.00001	0.70374	0.00007	0.70374	0.00007
LX1511@4	19.92	0.05705	0.00020	0.00681	0.00002	0.00010	0.00001	0.70335	0.00006	0.70335	0.00006
LX1511@6	19.92	0.05714	0.00017	0.00682	0.00002	0.00080	0.00003	0.70336	0.00007	0.70336	0.00007
LX1511@7	19.92	0.05695	0.00024	0.00680	0.00003	0.00010	0.00001	0.70380	0.00008	0.70380	0.00008
LX1511@8	19.92	0.05719	0.00027	0.00683	0.00003	0.00015	0.00001	0.70381	0.00007	0.70381	0.00007
LX1511@9	19.92	0.05724	0.00027	0.00683	0.00003	0.00010	0.00001	0.70374	0.00008	0.70374	0.00008
LX1511@10	19.92	0.05675	0.00020	0.00678	0.00002	0.00009	0.00001	0.70356	0.00008	0.70356	0.00008
LX1511@11	19.92	0.05675	0.00013	0.00678	0.00002	0.00019	0.00003	0.70309	0.00005	0.70309	0.00005
LX1511@12	19.92	0.05676	0.00014	0.00678	0.00002	0.00015	0.00001	0.70310	0.00005	0.70310	0.00005
LX1511@13	19.92	0.05665	0.00015	0.00676	0.00002	0.00012	0.00001	0.70326	0.00005	0.70326	0.00005
LX1511@14	19.92	0.05683	0.00013	0.00679	0.00001	0.00017	0.00001	0.70314	0.00006	0.70314	0.00006
LX1511@15	19.92	0.05685	0.00009	0.00679	0.00001	0.00012	0.00001	0.70296	0.00006	0.70296	0.00006
LX1511@16	19.92	0.05673	0.00027	0.00677	0.00003	0.00017	0.00001	0.70406	0.00009	0.70406	0.00009
LX1511@17	19.92	0.05728	0.00016	0.00684	0.00002	0.00010	0.00001	0.70334	0.00006	0.70334	0.00006
LX1511@18	19.92	0.05691	0.00012	0.00680	0.00001	0.00010	0.00000	0.70305	0.00004	0.70305	0.00004
LX1511@19	19.92	0.05692	0.00012	0.00680	0.00001	0.00023	0.00001	0.70311	0.00005	0.70311	0.00005
LX1511@20	19.92	0.05693	0.00015	0.00680	0.00002	0.00009	0.00001	0.70321	0.00006	0.70321	0.00006
LX1511@21	19.92	0.05673	0.00014	0.00677	0.00002	0.00075	0.00004	0.70311	0.00006	0.70311	0.00006
LX1511@22	19.92	0.05717	0.00029	0.00683	0.00003	0.00013	0.00002	0.70394	0.00008	0.70394	0.00008
LX1511@23	19.92	0.05690	0.00016	0.00679	0.00002	0.00009	0.00001	0.70312	0.00006	0.70312	0.00006
LX1511@24	19.92	0.05745	0.00025	0.00686	0.00003	0.00015	0.00001	0.70379	0.00008	0.70379	0.00008
LX1511@25	19.92	0.05708	0.00033	0.00682	0.00004	0.00018	0.00003	0.70415	0.00009	0.70415	0.00009
LX1511@26	19.92	0.05667	0.00033	0.00677	0.00004	0.00113	0.00006	0.70387	0.00009	0.70387	0.00009
LX1511@27	19.92	0.05721	0.00030	0.00683	0.00004	0.00014	0.00001	0.70409	0.00010	0.70409	0.00010
LX1511@28	19.92	0.05716	0.00017	0.00683	0.00002	0.00010	0.00001	0.70324	0.00005	0.70324	0.00005
Sample LX1525											
LX1525@1	16.19	0.05714	0.00027	0.00682	0.00003	0.00093	0.00010	0.70384	0.00007	0.70384	0.00007
LX1525@2	16.19	0.05679	0.00022	0.00678	0.00003	0.00044	0.00001	0.70358	0.00008	0.70358	0.00008
LX1525@3	16.19	0.05713	0.00016	0.00682	0.00002	0.00010	0.00001	0.70305	0.00005	0.70305	0.00005
LX1525@4	16.19	0.05669	0.00026	0.00677	0.00003	0.00009	0.00001	0.70367	0.00008	0.70367	0.00008
LX1525@5	16.19	0.05679	0.00034	0.00678	0.00004	0.00014	0.00002	0.70400	0.00009	0.70400	0.00009
LX1525@6	16.19	0.05712	0.00019	0.00682	0.00002	0.00014	0.00001	0.70336	0.00007	0.70336	0.00007
LX1525@7	16.19	0.05685	0.00013	0.00679	0.00002	0.00007	0.00001	0.70311	0.00006	0.70311	0.00006
LX1525@8	16.19	0.05725	0.00028	0.00684	0.00003	0.00011	0.00001	0.70400	0.00008	0.70400	0.00008
LX1525@9	16.19	0.05685	0.00010	0.00679	0.00001	0.00006	0.00000	0.70306	0.00005	0.70306	0.00005
LX1525@10	16.19	0.05708	0.00035	0.00682	0.00004	0.00012	0.00001	0.70421	0.00009	0.70421	0.00009
LX1525@11	16.19	0.05691	0.00009	0.00680	0.00001	0.00017	0.00002	0.70297	0.00005	0.70297	0.00005
LX1525@12	16.19	0.05683	0.00009	0.00679	0.00001	0.00006	0.00001	0.70286	0.00005	0.70286	0.00005
LX1525@13	16.19	0.05678	0.00009	0.00678	0.00001	0.00015	0.00001	0.70295	0.00005	0.70295	0.00005
LX1525@14	16.19	0.05705	0.00012	0.00681	0.00001	0.00013	0.00002	0.70316	0.00005	0.70316	0.00005
LX1525@15	16.19	0.05689	0.00014	0.00679	0.00002	0.00008	0.00001	0.70315	0.00006	0.70315	0.00006
LX1525@16	16.19	0.05720	0.00015	0.00683	0.00002	0.00008	0.00001	0.70306	0.00006	0.70306	0.00006
LX1525@17	16.19	0.05720	0.00028	0.00683	0.00003	0.00013	0.00001	0.70381	0.00008	0.70381	0.00008
LX1525@18	16.19	0.05675	0.00028	0.00678	0.00003	0.00013	0.00001	0.70400	0.00009	0.70400	0.00009

Table DR5 (***continued***)

Analysis spot	Age (Ma)	$^{84}Sr/^{86}Sr$	2σ	$^{84}Sr/^{88}Sr$	2σ	$^{87}Rb/^{86}Sr$	2σ	$^{87}Sr/^{86}Sr$	2σ	$^{87}Sr/^{86}Sr_i$	2σ
LX1525@19	16.19	0.05696	0.00028	0.00680	0.00003	0.00011	0.00001	0.70388	0.00008	0.70388	0.00008
LX1525@20	16.19	0.05695	0.00029	0.00680	0.00003	0.00016	0.00001	0.70387	0.00007	0.70387	0.00007
LX1525@21	16.19	0.05705	0.00024	0.00681	0.00003	0.00018	0.00001	0.70354	0.00007	0.70354	0.00007
LX1525@22	16.19	0.05703	0.00010	0.00681	0.00001	0.00010	0.00002	0.70297	0.00005	0.70297	0.00005
LX1525@23	16.19	0.05698	0.00030	0.00680	0.00004	0.00014	0.00001	0.70417	0.00008	0.70417	0.00008
LX1525@24	16.19	0.05721	0.00015	0.00683	0.00002	0.00007	0.00001	0.70317	0.00005	0.70317	0.00005
LX1525@25	16.19	0.05704	0.00026	0.00681	0.00003	0.00011	0.00001	0.70383	0.00008	0.70383	0.00008
LX1525@26	16.19	0.05684	0.00008	0.00679	0.00001	0.00014	0.00001	0.70279	0.00005	0.70279	0.00005
LX1525@27	16.19	0.05681	0.00005	0.00678	0.00001	0.00004	0.00000	0.70268	0.00003	0.70268	0.00003
LX1525@28	16.19	0.05687	0.00009	0.00679	0.00001	0.00005	0.00000	0.70289	0.00005	0.70289	0.00005
LX1525@29	16.19	0.05677	0.00009	0.00678	0.00001	0.00005	0.00000	0.70288	0.00005	0.70288	0.00005
LX1525@30	16.19	0.05684	0.00016	0.00679	0.00002	0.00007	0.00001	0.70328	0.00006	0.70328	0.00006
LX1525@31	16.19	0.05689	0.00008	0.00679	0.00001	0.00004	0.00000	0.70278	0.00005	0.70278	0.00005
LX1525@32	16.19	0.05671	0.00029	0.00677	0.00003	0.00009	0.00001	0.70380	0.00008	0.70380	0.00008
LX1525@33	16.19	0.05699	0.00008	0.00680	0.00001	0.00048	0.00001	0.70282	0.00004	0.70282	0.00004
LX1525@34	16.19	0.05682	0.00011	0.00678	0.00001	0.00005	0.00000	0.70284	0.00005	0.70284	0.00005
LX1525@35	16.19	0.05698	0.00011	0.00680	0.00001	0.00007	0.00000	0.70291	0.00004	0.70291	0.00004

- $^{87}Sr/^{86}Sri = {}^{87}Sr/^{86}Sr_{sample} - {}^{87}Rb/^{86}Sr_{sample} \times (e^{\lambda t}-1)$

- $\lambda = 1.42 \times 10^{-11}$ yr^{-1} (Steiger and Jäger, 1977), t = crystallization time of perovskite.

Table DR6 **Sm-Nd isotopic data of AFK standard and perovskites from the west Qinling kamafugites**

Analysis spot	Age (Ma)	$^{147}Sm/^{144}Nd$	2σ	$^{145}Nd/^{144}Nd$	2σ	$^{143}Nd/^{144}Nd$	2σ	$^{143}Nd/^{144}Nd(t)$	$\varepsilon_{Nd}(t)$	2σ
AFK Standard										
AFK@1	379	0.07638	0.00018	0.34835	0.00002	0.51258	0.00004	0.51239	4.7	0.7
AFK@2	379	0.07536	0.00009	0.34839	0.00002	0.51260	0.00003	0.51241	5.2	0.7
AFK@3	379	0.07471	0.00010	0.34838	0.00002	0.51260	0.00003	0.51242	5.2	0.7
AFK@4	379	0.07464	0.00010	0.34836	0.00002	0.51261	0.00004	0.51243	5.5	0.7
AFK@5	379	0.07486	0.00011	0.34838	0.00002	0.51260	0.00003	0.51242	5.2	0.6
AFK@6	379	0.07544	0.00008	0.34839	0.00002	0.51263	0.00004	0.51244	5.7	0.7
AFK@7	379	0.07449	0.00010	0.34838	0.00002	0.51260	0.00003	0.51242	5.2	0.6
AFK@8	379	0.06935	0.00005	0.34839	0.00002	0.51260	0.00003	0.51243	5.5	0.6
AFK@9	379	0.07735	0.00005	0.34839	0.00002	0.51264	0.00003	0.51245	5.9	0.6
AFK@10	379	0.08288	0.00009	0.34836	0.00002	0.51263	0.00003	0.51243	5.4	0.7
AFK@11	379	0.07680	0.00022	0.34836	0.00002	0.51263	0.00004	0.51244	5.7	0.7
AFK@12	379	0.07551	0.00014	0.34839	0.00002	0.51263	0.00004	0.51245	5.8	0.7
AFK@13	379	0.07951	0.00009	0.34840	0.00002	0.51261	0.00003	0.51242	5.2	0.7
AFK@14	379	0.07956	0.00009	0.34838	0.00002	0.51260	0.00003	0.51241	5.0	0.7
AFK@15	379	0.07967	0.00009	0.34835	0.00002	0.51259	0.00003	0.51240	4.8	0.7
AFK@16	379	0.07946	0.00009	0.34835	0.00002	0.51259	0.00003	0.51239	4.8	0.6
AFK@17	379	0.07948	0.00009	0.34838	0.00002	0.51260	0.00003	0.51240	4.9	0.7
AFK@18	379	0.07642	0.00013	0.34836	0.00002	0.51259	0.00003	0.51240	4.9	0.6
AFK@19	379	0.08342	0.00007	0.34837	0.00002	0.51262	0.00003	0.51242	5.2	0.6
AFK@20	379	0.08473	0.00007	0.34838	0.00002	0.51263	0.00003	0.51242	5.3	0.6
AFK@21	379	0.07964	0.00012	0.34834	0.00002	0.51261	0.00003	0.51241	5.1	0.6
AFK@22	379	0.07030	0.00004	0.34838	0.00002	0.51259	0.00003	0.51242	5.2	0.6
AFK@23	379	0.08164	0.00012	0.34838	0.00002	0.51260	0.00003	0.51240	4.9	0.6
AFK@24	379	0.08046	0.00013	0.34840	0.00002	0.51261	0.00003	0.51241	5.1	0.5
AFK@25	379	0.07537	0.00009	0.34835	0.00002	0.51261	0.00003	0.51242	5.3	0.5
AFK@26	379	0.08592	0.00004	0.34838	0.00002	0.51261	0.00004	0.51240	4.9	0.7
AFK@27	379	0.08350	0.00016	0.34837	0.00002	0.51261	0.00003	0.51240	5.0	0.6
AFK@28	379	0.07971	0.00005	0.34838	0.00002	0.51261	0.00003	0.51241	5.2	0.6
AFK@29	379	0.07528	0.00008	0.34839	0.00002	0.51261	0.00004	0.51243	5.4	0.7
AFK@30	379	0.07191	0.00004	0.34837	0.00002	0.51264	0.00003	0.51247	6.2	0.6
AFK@31	379	0.07490	0.00010	0.34838	0.00002	0.51263	0.00003	0.51244	5.8	0.6
AFK@32	379	0.06856	0.00009	0.34839	0.00002	0.51257	0.00003	0.51240	4.8	0.6
~~AFK@33~~	~~379~~	~~0.08334~~	~~0.00005~~	~~0.34841~~	~~0.00002~~	~~0.51265~~	~~0.00004~~	~~0.51245~~	~~5.8~~	~~0.7~~
AFK@34	379	0.06882	0.00004	0.34840	0.00002	0.51259	0.00003	0.51242	5.3	0.6
AFK@35	379	0.08206	0.00007	0.34840	0.00002	0.51262	0.00004	0.51242	5.2	0.7
AFK@36	379	0.07998	0.00010	0.34838	0.00002	0.51262	0.00004	0.51243	5.4	0.7
~~AFK@37~~	~~379~~	~~0.06724~~	~~0.00005~~	~~0.34839~~	~~0.00002~~	~~0.51254~~	~~0.00003~~	~~0.51238~~	~~4.5~~	~~0.6~~
~~AFK@38~~	~~379~~	~~0.07726~~	~~0.00010~~	~~0.34839~~	~~0.00002~~	~~0.51255~~	~~0.00004~~	~~0.51236~~	~~4.1~~	~~0.8~~
AFK@39	379	0.07169	0.00016	0.34840	0.00002	0.51258	0.00003	0.51240	4.9	0.6
~~AFK@40~~	~~379~~	~~0.07138~~	~~0.00007~~	~~0.34840~~	~~0.00002~~	~~0.51255~~	~~0.00003~~	~~0.51237~~	~~4.3~~	~~0.7~~
AFK@41	379	0.07315	0.00009	0.34839	0.00002	0.51257	0.00004	0.51239	4.6	0.7
AFK@42	379	0.07482	0.00022	0.34839	0.00002	0.51261	0.00004	0.51243	5.4	0.8
AFK@43	379	0.08207	0.00006	0.34834	0.00002	0.51261	0.00003	0.51241	5.0	0.6
AFK@44	379	0.08046	0.00004	0.34837	0.00002	0.51259	0.00003	0.51239	4.7	0.6
AFK@45	379	0.08003	0.00006	0.34837	0.00002	0.51261	0.00004	0.51242	5.2	0.7
AFK@46	379	0.07361	0.00005	0.34842	0.00002	0.51258	0.00003	0.51240	4.9	0.6
AFK@47	379	0.07864	0.00011	0.34838	0.00002	0.51260	0.00003	0.51241	5.1	0.7
AFK@48	379	0.08224	0.00007	0.34836	0.00002	0.51262	0.00003	0.51242	5.2	0.6
AFK@49	379	0.07954	0.00016	0.34835	0.00002	0.51262	0.00004	0.51242	5.4	0.7
AFK@50	379	0.06825	0.00016	0.34838	0.00002	0.51259	0.00003	0.51243	5.4	0.7
AFK@51	379	0.08240	0.00006	0.34839	0.00002	0.51262	0.00003	0.51242	5.2	0.6
AFK@52	379	0.07618	0.00006	0.34838	0.00002	0.51256	0.00003	0.51238	4.4	0.6
AFK@53	379	0.08091	0.00005	0.34840	0.00002	0.51260	0.00003	0.51240	4.9	0.6
AFK@54	379	0.07990	0.00019	0.34839	0.00002	0.51261	0.00004	0.51241	5.1	0.7
AFK@55	379	0.08145	0.00006	0.34839	0.00002	0.51259	0.00003	0.51239	4.7	0.6

Table DR6 (*continued*)

Analysis spot	Age (Ma)	$^{147}Sm/^{144}Nd$	2σ	$^{145}Nd/^{144}Nd$	2σ	$^{143}Nd/^{144}Nd$	2σ	$^{143}Nd/^{144}Nd(t)$	$\varepsilon_{Nd}(t)$	2σ
Sample LX1506										
LX1506@1	16.58	0.08512	0.00011	0.34835	0.00003	0.51289	0.00004	0.51288	5.2	0.9
LX1506@2	16.58	0.09099	0.00020	0.34833	0.00003	0.51288	0.00005	0.51287	4.9	0.9
LX1506@3	16.58	0.09710	0.00019	0.34837	0.00003	0.51283	0.00005	0.51282	3.9	0.9
LX1506@4	16.58	0.09044	0.00026	0.34839	0.00003	0.51288	0.00004	0.51287	4.9	0.9
LX1506@5	16.58	0.09765	0.00020	0.34833	0.00003	0.51287	0.00005	0.51286	4.8	1.0
LX1506@6	16.58	0.08935	0.00011	0.34837	0.00003	0.51275	0.00005	0.51274	2.5	1.0
LX1506@7	16.58	0.10118	0.00027	0.34833	0.00004	0.51278	0.00006	0.51277	2.9	1.1
LX1506@8	16.58	0.09195	0.00011	0.34837	0.00002	0.51279	0.00005	0.51278	3.2	0.9
LX1506@9	16.58	0.09114	0.00013	0.34833	0.00003	0.51288	0.00005	0.51287	4.9	1.0
LX1506@10	16.58	0.09416	0.00009	0.34833	0.00003	0.51282	0.00005	0.51281	3.8	0.9
LX1506@11	16.58	0.09051	0.00012	0.34837	0.00003	0.51286	0.00004	0.51285	4.5	0.8
LX1506@12	16.58	0.09220	0.00015	0.34843	0.00004	0.51270	0.00006	0.51269	1.5	1.2
LX1506@13	16.58	0.09214	0.00028	0.34832	0.00003	0.51280	0.00005	0.51279	3.3	0.9
LX1506@14	16.58	0.09212	0.00013	0.34836	0.00003	0.51281	0.00005	0.51280	3.7	0.9
LX1506@15	16.58	0.09739	0.00022	0.34838	0.00003	0.51301	0.00006	0.51300	7.5	1.2
LX1506@16	16.58	0.09370	0.00031	0.34841	0.00003	0.51281	0.00004	0.51280	3.7	0.8
LX1506@17	16.58	0.08976	0.00015	0.34839	0.00002	0.51280	0.00004	0.51279	3.3	0.8
LX1506@18	16.58	0.09855	0.00013	0.34839	0.00003	0.51279	0.00005	0.51277	3.1	0.9
LX1506@19	16.58	0.07955	0.00004	0.34838	0.00002	0.51282	0.00003	0.51281	3.8	0.5
LX1506@20	16.58	0.08754	0.00010	0.34837	0.00003	0.51284	0.00004	0.51283	4.1	0.8
LX1506@21	16.58	0.08930	0.00012	0.34838	0.00002	0.51282	0.00004	0.51281	3.9	0.8
LX1506@22	16.58	0.09093	0.00011	0.34837	0.00002	0.51281	0.00004	0.51280	3.5	0.8
LX1506@23	16.58	0.09387	0.00008	0.34835	0.00003	0.51281	0.00005	0.51280	3.6	0.9
LX1506@24	16.58	0.08801	0.00007	0.34838	0.00003	0.51277	0.00004	0.51276	2.8	0.8
LX1506@25	16.58	0.08703	0.00032	0.34836	0.00002	0.51282	0.00004	0.51281	3.7	0.7
LX1506@26	16.58	0.08769	0.00008	0.34836	0.00002	0.51284	0.00004	0.51283	4.1	0.8
LX1506@27	16.58	0.08999	0.00011	0.34838	0.00003	0.51280	0.00004	0.51279	3.4	0.8
LX1506@28	16.58	0.09014	0.00050	0.34837	0.00002	0.51279	0.00004	0.51278	3.1	0.8
LX1506@29	16.58	0.10680	0.00016	0.34834	0.00003	0.51281	0.00005	0.51280	3.6	1.0
LX1506@30	16.58	0.09608	0.00008	0.34835	0.00003	0.51284	0.00005	0.51282	4.1	0.9
LX1506@31	16.58	0.10576	0.00017	0.34835	0.00003	0.51282	0.00006	0.51281	3.8	1.1
LX1506@32	16.58	0.08608	0.00011	0.34837	0.00002	0.51265	0.00003	0.51265	0.6	0.6
LX1506@33	16.58	0.08951	0.00018	0.34835	0.00003	0.51279	0.00004	0.51279	3.3	0.9
LX1506@34	16.58	0.11017	0.00030	0.34835	0.00003	0.51280	0.00004	0.51279	3.3	0.8
LX1506@35	16.58	0.11426	0.00023	0.34831	0.00004	0.51287	0.00007	0.51286	4.8	1.4
LX1506@36	16.58	0.08327	0.00007	0.34836	0.00003	0.51281	0.00004	0.51280	3.6	0.9
Sample LX1508										
LX1508@1	20.35	0.09661	0.00012	0.34836	0.00003	0.51286	0.00006	0.51285	4.6	1.1
LX1508@2	20.35	0.09787	0.00028	0.34836	0.00004	0.51273	0.00006	0.51272	2.1	1.1
LX1508@3	20.35	0.09564	0.00027	0.34832	0.00003	0.51279	0.00005	0.51277	3.2	0.9
LX1508@4	20.35	0.09964	0.00020	0.34838	0.00003	0.51285	0.00006	0.51284	4.4	1.2
LX1508@5	20.35	0.09226	0.00030	0.34832	0.00003	0.51282	0.00005	0.51280	3.7	1.1
LX1508@6	20.35	0.09862	0.00066	0.34838	0.00004	0.51288	0.00005	0.51287	5.0	1.1
LX1508@7	20.35	0.13104	0.00024	0.34829	0.00006	0.51273	0.00009	0.51271	2.0	1.7
LX1508@8	20.35	0.09706	0.00019	0.34835	0.00004	0.51276	0.00005	0.51275	2.7	1.0
LX1508@9	20.35	0.10211	0.00023	0.34832	0.00004	0.51272	0.00005	0.51271	1.9	1.0
LX1508@10	20.35	0.10750	0.00036	0.34835	0.00004	0.51281	0.00007	0.51279	3.5	1.5
LX1508@11	20.35	0.11320	0.00138	0.34834	0.00004	0.51276	0.00007	0.51274	2.6	1.4
LX1508@12	20.35	0.09495	0.00021	0.34838	0.00003	0.51282	0.00006	0.51281	3.8	1.1
LX1508@13	20.35	0.09621	0.00039	0.34830	0.00004	0.51290	0.00006	0.51289	5.5	1.1
LX1508@14	20.35	0.11258	0.00036	0.34840	0.00004	0.51285	0.00007	0.51283	4.3	1.3
LX1508@15	20.35	0.09314	0.00012	0.34838	0.00003	0.51288	0.00005	0.51287	5.0	1.0
LX1508@16	20.35	0.09071	0.00014	0.34836	0.00003	0.51278	0.00005	0.51277	3.1	0.9
LX1508@17	20.35	0.14249	0.00030	0.34836	0.00007	0.51265	0.00013	0.51264	0.5	2.4

Table DR6 (*continued*)

Analysis spot	Age (Ma)	$^{147}Sm/^{144}Nd$	2σ	$^{145}Nd/^{144}Nd$	2σ	$^{143}Nd/^{144}Nd$	2σ	$^{143}Nd/^{144}Nd(t)$	$\varepsilon_{Nd}(t)$	2σ
LX1508@18	20.35	0.14842	0.00043	0.34832	0.00007	0.51278	0.00013	0.51276	2.9	2.4
LX1508@19	20.35	0.09681	0.00036	0.34832	0.00003	0.51283	0.00006	0.51282	4.0	1.1
LX1508@20	20.35	0.11083	0.00037	0.34835	0.00004	0.51279	0.00006	0.51277	3.1	1.2
LX1508@21	20.35	0.10939	0.00036	0.34838	0.00004	0.51275	0.00007	0.51273	2.4	1.3
LX1508@22	20.35	0.10636	0.00021	0.34841	0.00005	0.51285	0.00006	0.51283	4.3	1.2
LX1508@23	20.35	0.12131	0.00037	0.34839	0.00005	0.51277	0.00007	0.51275	2.7	1.4
LX1508@24	20.35	0.12416	0.00080	0.34836	0.00005	0.51268	0.00008	0.51266	1.0	1.5
LX1508@25	20.35	0.09406	0.00008	0.34837	0.00003	0.51280	0.00005	0.51279	3.4	1.0
LX1508@26	20.35	0.12490	0.00036	0.34833	0.00005	0.51274	0.00008	0.51272	2.1	1.6
LX1508@27	20.35	0.09611	0.00046	0.34837	0.00003	0.51278	0.00005	0.51277	3.1	1.0
Sample LX1511										
LX1511@1	19.92	0.16934	0.00057	0.34829	0.00004	0.51280	0.00008	0.51277	3.1	1.6
LX1511@2	19.92	0.15551	0.00012	0.34833	0.00003	0.51288	0.00005	0.51286	4.7	1.0
LX1511@3	19.92	0.15417	0.00036	0.34834	0.00002	0.51276	0.00005	0.51274	2.6	0.9
LX1511@4	19.92	0.17999	0.00018	0.34834	0.00004	0.51279	0.00006	0.51277	3.1	1.2
LX1511@6	19.92	0.15622	0.00045	0.34840	0.00003	0.51283	0.00005	0.51281	3.9	0.9
LX1511@7	19.92	0.16165	0.00034	0.34832	0.00003	0.51287	0.00006	0.51285	4.7	1.1
LX1511@8	19.92	0.14792	0.00056	0.34831	0.00003	0.51278	0.00005	0.51277	3.0	1.0
LX1511@9	19.92	0.16627	0.00017	0.34838	0.00003	0.51285	0.00005	0.51283	4.2	1.0
LX1511@10	19.92	0.18130	0.00014	0.34833	0.00004	0.51275	0.00006	0.51273	2.3	1.2
LX1511@11	19.92	0.16331	0.00036	0.34838	0.00003	0.51283	0.00006	0.51281	3.8	1.2
LX1511@12	19.92	0.16952	0.00034	0.34836	0.00004	0.51294	0.00006	0.51292	6.1	1.1
LX1511@13	19.92	0.17225	0.00028	0.34838	0.00004	0.51290	0.00006	0.51288	5.2	1.2
LX1511@14	19.92	0.16216	0.00011	0.34836	0.00003	0.51282	0.00005	0.51280	3.6	1.0
LX1511@15	19.92	0.15673	0.00012	0.34841	0.00003	0.51277	0.00005	0.51275	2.7	1.0
LX1511@16	19.92	0.13846	0.00031	0.34831	0.00003	0.51283	0.00004	0.51281	3.9	0.8
LX1511@17	19.92	0.16902	0.00014	0.34836	0.00004	0.51275	0.00005	0.51273	2.2	1.1
LX1511@18	19.92	0.16684	0.00044	0.34821	0.00006	0.51281	0.00006	0.51279	3.4	1.1
LX1511@19	19.92	0.15715	0.00084	0.34828	0.00004	0.51290	0.00006	0.51288	5.2	1.2
LX1511@20	19.92	0.17422	0.00029	0.34839	0.00004	0.51283	0.00006	0.51281	3.8	1.1
LX1511@21	19.92	0.16313	0.00020	0.34838	0.00003	0.51285	0.00006	0.51283	4.2	1.2
LX1511@22	19.92	0.11554	0.00063	0.34839	0.00001	0.51281	0.00003	0.51279	3.5	0.6
LX1511@23	19.92	0.16554	0.00014	0.34834	0.00003	0.51272	0.00006	0.51270	1.7	1.3
LX1511@24	19.92	0.15165	0.00080	0.34838	0.00002	0.51277	0.00004	0.51275	2.7	0.7
LX1511@25	19.92	0.15491	0.00081	0.34836	0.00003	0.51288	0.00004	0.51286	4.8	0.8
LX1511@26	19.92	0.09805	0.00065	0.34835	0.00001	0.51282	0.00002	0.51281	3.9	0.4
LX1511@27	19.92	0.13328	0.00029	0.34842	0.00002	0.51276	0.00003	0.51275	2.6	0.6
LX1511@28	19.92	0.14946	0.00049	0.34836	0.00004	0.51280	0.00005	0.51279	3.4	1.0
Sample LX1525										
LX1525@1	16.19	0.10220	0.00013	0.34832	0.00003	0.51289	0.00004	0.51288	5.2	0.8
LX1525@2	16.19	0.10599	0.00008	0.34835	0.00002	0.51278	0.00004	0.51277	3.0	0.7
LX1525@3	16.19	0.10256	0.00015	0.34835	0.00002	0.51281	0.00003	0.51280	3.5	0.6
LX1525@4	16.19	0.10453	0.00016	0.34838	0.00002	0.51281	0.00003	0.51280	3.5	0.7
LX1525@5	16.19	0.10179	0.00011	0.34838	0.00002	0.51283	0.00003	0.51282	4.0	0.6
LX1525@6	16.19	0.10629	0.00014	0.34836	0.00002	0.51280	0.00003	0.51279	3.4	0.7
LX1525@7	16.19	0.11451	0.00021	0.34836	0.00002	0.51281	0.00004	0.51280	3.5	0.8
LX1525@8	16.19	0.10985	0.00091	0.34836	0.00002	0.51282	0.00004	0.51281	3.7	0.7
LX1525@9	16.19	0.12798	0.00040	0.34832	0.00003	0.51282	0.00005	0.51280	3.7	1.0
LX1525@10	16.19	0.11206	0.00016	0.34837	0.00002	0.51282	0.00003	0.51281	3.8	0.7
LX1525@11	16.19	0.12044	0.00016	0.34836	0.00003	0.51287	0.00005	0.51286	4.7	0.9
LX1525@12	16.19	0.13542	0.00100	0.34829	0.00004	0.51285	0.00007	0.51284	4.3	1.3
LX1525@13	16.19	0.11045	0.00022	0.34834	0.00002	0.51279	0.00004	0.51277	3.1	0.8
LX1525@14	16.19	0.11944	0.00026	0.34834	0.00003	0.51285	0.00005	0.51283	4.2	0.9
LX1525@15	16.19	0.10403	0.00009	0.34838	0.00002	0.51281	0.00004	0.51280	3.5	0.7

Table DR6 (***continued***)

Analysis spot	Age (Ma)	$^{147}Sm/^{144}Nd$	2σ	$^{145}Nd/^{144}Nd$	2σ	$^{143}Nd/^{144}Nd$	2σ	$^{143}Nd/^{144}Nd(t)$	$\varepsilon_{Nd}(t)$	2σ
LX1525@16	16.19	0.12381	0.00022	0.34836	0.00003	0.51297	0.00006	0.51295	6.6	1.1
LX1525@17	16.19	0.09896	0.00017	0.34837	0.00002	0.51279	0.00003	0.51278	3.2	0.6
LX1525@18	16.19	0.10763	0.00034	0.34835	0.00002	0.51283	0.00004	0.51282	3.9	0.7
LX1525@19	16.19	0.10167	0.00036	0.34840	0.00002	0.51278	0.00003	0.51277	3.0	0.6
LX1525@20	16.19	0.11123	0.00012	0.34835	0.00002	0.51284	0.00004	0.51283	4.1	0.7
LX1525@21	16.19	0.10611	0.00054	0.34834	0.00002	0.51282	0.00003	0.51281	3.7	0.7
LX1525@22	16.19	0.10398	0.00016	0.34835	0.00002	0.51279	0.00003	0.51278	3.1	0.6
LX1525@23	16.19	0.11078	0.00081	0.34834	0.00003	0.51286	0.00004	0.51285	4.5	0.7
LX1525@24	16.19	0.11174	0.00005	0.34835	0.00002	0.51285	0.00003	0.51284	4.4	0.7
LX1525@25	16.19	0.10883	0.00024	0.34839	0.00002	0.51283	0.00003	0.51281	3.8	0.7
LX1525@26	16.19	0.11777	0.00040	0.34836	0.00002	0.51282	0.00004	0.51281	3.7	0.8
LX1525@27	16.19	0.11846	0.00007	0.34838	0.00003	0.51280	0.00004	0.51279	3.3	0.8
LX1525@28	16.19	0.11335	0.00008	0.34839	0.00002	0.51282	0.00004	0.51280	3.6	0.7
LX1525@29	16.19	0.11254	0.00006	0.34837	0.00002	0.51282	0.00004	0.51281	3.8	0.7
LX1525@30	16.19	0.11358	0.00023	0.34835	0.00002	0.51283	0.00003	0.51282	3.9	0.7
LX1525@31	16.19	0.11891	0.00045	0.34840	0.00002	0.51282	0.00004	0.51281	3.7	0.8
LX1525@32	16.19	0.10831	0.00012	0.34837	0.00002	0.51275	0.00004	0.51274	2.4	0.8
LX1525@33	16.19	0.11854	0.00039	0.34837	0.00003	0.51276	0.00004	0.51275	2.5	0.7
LX1525@34	16.19	0.11023	0.00012	0.34839	0.00002	0.51283	0.00003	0.51282	3.9	0.7
LX1525@35	16.19	0.13444	0.00022	0.34836	0.00003	0.51283	0.00005	0.51281	3.8	1.0

- $^{143}Nd/^{144}Nd(t) = {}^{143}Nd/^{144}Nd_{sample} - {}^{147}Sm/^{144}Nd_{sample} \times (e^{\lambda t}-1)$

- $\varepsilon_{Nd}(t) = \left[\frac{^{143}Nd/^{144}Nd_{sample} - {}^{147}Sm/^{144}Nd_{sample} \times (e^{\lambda t}-1)}{^{143}Nd/^{144}Nd_{CHUR} - {}^{147}Sm/^{144}Nd_{CHUR} \times (e^{\lambda t}-1)} - 1\right] \times 10^4$

- $\lambda = 6.54 \times 10^{-12}$ yr^{-1} (Lugmair and Marti, 1978), $^{147}Sm/^{144}Nd_{CHUR} = 0.1967$ (Jacobsen and Wasserburg, 1980), $^{143}Nd/^{144}Nd_{CHUR} = 0.512638$ (Goldstein et al., 1984). t = crystallization time of perovskite.

Table DR7 Whole-rock Sr-Nd isotopic data of kamafugites and entrained mantle xenoliths

Sample	Age (Ma)	Lithology	Rb (ppm)	Sr (ppm)	$^{87}Sr/^{86}Sr$	$^{87}Sr/^{86}Sr_i$	Sm (ppm)	Nd (ppm)	$^{143}Nd/^{144}Nd$	$\varepsilon_{Nd}(t)$	Data source
SW6*	18	Kamafugite	68.7	1842	0.703974	0.7039	18.7	102	0.512008	3.56	Dong et al., 2008
F1*	18	Kamafugite	23.9	1728	0.704419	0.7044	19.4	109	0.512037	4.13	Dong et al., 2008
F4*	18	Kamafugite	28.5	1546	0.704330	0.7043	19.3	109	0.512047	4.33	Dong et al., 2008
F8*	18	Kamafugite	22.0	1811	0.704461	0.7045	19.4	110	0.512042	4.23	Dong et al., 2008
F17*	18	Kamafugite	26.0	1656	0.704726	0.7047	18.8	106	0.512050	4.39	Dong et al., 2008
F21*	18	Kamafugite	23.5	1940	0.704500	0.7045	18.3	104	0.512048	4.35	Dong et al., 2008
HT7*	18	Kamafugite	71.2	1552	0.703878	0.7038	15.9	85.3	0.512088	5.12	Dong et al., 2008
HT11*	18	Kamafugite	69.2	1601	0.703878	0.7038	17.0	89.4	0.512094	5.23	Dong et al., 2008
DS1*	18	Kamafugite	80.9	1682	0.704172	0.7041	19.5	106	0.512048	4.34	Dong et al., 2008
XD20*	18	Kamafugite	53.0	1900	0.703880	0.7039	22.8	124	0.512049	4.36	Dong et al., 2008
JK6*	18	Kamafugite	94.5	1742	0.703975	0.7039	19.6	101	0.512052	4.40	Dong et al., 2008
JK7*	18	Kamafugite	24.5	1602	0.704549	0.7045	18.7	107	0.512052	4.43	Dong et al., 2008
ND17*	18	Kamafugite	6.18	269	0.704660	0.7046	3.12	17.9	0.512058	4.55	Dong et al., 2008
ND20*	18	Kamafugite	93.7	1699	0.703985	0.7039	19.5	102	0.512007	3.52	Dong et al., 2008
ND23*	18	Kamafugite	81.3	1801	0.704121	0.7041	20.1	105	0.512076	4.88	Dong et al., 2008
DS0305A	18	Kamafugite	131	1913	0.704030	0.7040	27.2	147	0.512830	3.95	Yu et al., 2009
DS0305B	18	Kamafugite	130	1862	0.704110	0.7041	26.3	131	0.512752	2.40	Yu et al., 2009
BGL0315	18	Kamafugite	31.2	1544	0.704730	0.7047	16.8	77.9	0.512943	6.10	Yu et al., 2009
BGL0314	18	Kamafugite	41.8	1447	0.704330	0.7043	15.3	75.6	0.512785	3.04	Yu et al., 2009
CZ0303A	18	Kamafugite	125	1726	0.707490	0.7074	22.2	108	0.512695	1.28	Yu et al., 2009
CZ0303B	18	Kamafugite	125	1726	0.704510	0.7045	22.2	108	0.512738	2.12	Yu et al., 2009
WZB0306A	18	Kamafugite	43.6	2313	0.705050	0.7050	26.7	129	0.512770	2.75	Yu et al., 2009
WZB0306B	18	Kamafugite	59.1	1921	0.705210	0.7052	25.3	121	0.512775	2.84	Yu et al., 2009
PJS0310	18	Kamafugite	36.9	1718	0.704130	0.7041	18.5	83.3	0.512764	2.60	Yu et al., 2009
HYS0316	18	Kamafugite	35.6	1135	0.704680	0.7047	15.9	73.7	0.512759	2.52	Yu et al., 2009
GJS_0320	18	Kamafugite	22.6	1213	0.704769	0.7048	15.7	73.4	0.512764	2.61	Yu et al., 2009
8617	18	Kamafugite	61.8	1570	0.704120	0.7041	15.6	79.6	0.512782	2.99	Yu et al., 2004
8752	18	Kamafugite	60.1	1284	0.704250	0.7042	10.8	62.0	0.512880	4.93	Yu et al., 2004
8628	18	Kamafugite	66.1	1393	0.704380	0.7043	18.6	101	0.512794	3.24	Yu et al., 2001
9113	18	Kamafugite	69.0	1003	0.705250	0.7052	20.5	113	0.512911	5.53	Yu et al., 2001
2003	18	Kamafugite	19.6	2180	0.703830	0.7038	16.9	98.3	0.512845	4.25	Yu et al., 2004
2011	18	Kamafugite	51.9	1620	0.704290	0.7043	17.0	96.3	0.512887	5.06	Yu et al., 2004
LN10-001	18	Kamafugite	30.5	1367	0.704336	0.7043	18.0	102	0.512838	4.11	Guo et al., 2014
LN10-002	18	Kamafugite	37.4	1299	0.704281	0.7043	18.2	103	0.512853	4.40	Guo et al., 2014
LN10-015	18	Kamafugite	34.4	1526	0.704779	0.7048	18.7	107	0.512829	3.94	Guo et al., 2014
LN10-029	18	Kamafugite	69.3	1582	0.703996	0.7040	17.9	96.9	0.512856	4.45	Guo et al., 2014
9118	18	Kamafugite	56.3	1722	0.704190	0.7042	12.1	64.3	0.512768	2.73	Yu et al., 2001
9126	18	Kamafugite	57.9	954	0.704340	0.7043	15.0	84.3	0.512773	2.84	Yu et al., 2001
2004	18	Kamafugite	160	1060	0.704430	0.7043	13.6	77.9	0.512894	5.20	Yu et al., 2004
2008	18	Kamafugite	86.4	1410	0.706230	0.7062	18.5	106	0.512924	5.79	Yu et al., 2004
2009	18	Kamafugite	43.8	1350	0.704500	0.7045	15.1	88.6	0.512831	3.98	Yu et al., 2004
2014	18	Kamafugite			0.705400	0.7054			0.512780	2.80	Yu et al., 2004
2016	18	Kamafugite			0.709450	0.7094			0.512464	-3.40	Yu et al., 2004
2017	18	Kamafugite			0.707480	0.7075			0.512911	5.30	Yu et al., 2004
2104	18	Kamafugite			0.704030	0.7040			0.512889	4.90	Yu et al., 2004
2107	18	Kamafugite			0.705160	0.7051			0.512705	1.30	Yu et al., 2004
2108	18	Kamafugite			0.705160	0.7052			0.512787	2.90	Yu et al., 2004
2112	18	Kamafugite			0.704010	0.7040			0.512858	4.30	Yu et al., 2004
2115	18	Kamafugite			0.709240	0.7092			0.512404	-4.60	Yu et al., 2004
14HT01	18	Kamafugite	43.4	1409	0.704082	0.7041	15.5	80.5	0.512891	5.12	Dai et al., 2017
14HT03	18	Kamafugite	79.2	1806	0.704167	0.7041	16.6	87.3	0.512873	4.77	Dai et al., 2017
14HT05	18	Kamafugite	89.3	1685	0.703835	0.7038	16.6	86.5	0.512855	4.42	Dai et al., 2017
14HT08	18	Kamafugite	62.1	1700	0.703776	0.7037	15.3	80.6	0.512878	4.87	Dai et al., 2017
14HT10	18	Kamafugite	74.8	1691	0.703880	0.7038	16.4	87.1	0.512863	4.58	Dai et al., 2017
14LX04	18	Kamafugite	81.1	1304	0.704316	0.7043	13.1	70.6	0.512817	3.69	Dai et al., 2017
14FS03	18	Kamafugite	31.7	1692	0.704747	0.7047	17.1	95.4	0.512818	3.71	Dai et al., 2017

Table DR7 (***continued***)

Sample	**Age (Ma)**	**Lithology**	**Rb (ppm)**	**Sr (ppm)**	**$^{87}Sr/^{86}Sr$**	**$^{87}Sr/^{86}Sr_i$**	**Sm (ppm)**	**Nd (ppm)**	**$^{143}Nd/^{144}Nd$**	**$\varepsilon_{Nd}(t)$**	**Data source**
14FS17	18	Kamafugite	43.7	1409	0.704435	0.7044	14.7	83.2	0.512805	3.46	Dai et al., 2017
14FS18	18	Kamafugite	50.4	1483	0.704270	0.7042	14.9	84.1	0.512801	3.39	Dai et al., 2017
14FS23	18	Kamafugite	34.7	1399	0.704262	0.7042	17.3	95.1	0.512807	3.50	Dai et al., 2017
14FS25	18	Kamafugite	20.8	2035	0.704041	0.7040	17.5	96.5	0.512803	3.42	Dai et al., 2017
HT08-1	18	Grt lherzolite	7.14	115	0.704525	0.7045	1.04	5.35	0.512707	1.53	Su et al., 2012
HT08-2	18	Grt lherzolite	12.5	56.3	0.705469	0.7053	0.48	2.14	0.512752	2.36	Su et al., 2012
HT08-9	18	Grt lherzolite	6.41	37.7	0.704410	0.7043	0.37	1.79	0.512800	3.33	Su et al., 2012
HT08-11	18	Grt lherzolite	6.93	132	0.704192	0.7042	1.30	7.08	0.512957	6.42	Su et al., 2012
HT08-6	18	Spl-Grt lherzolite	3.91	94.0	0.704958	0.7049	0.75	4.01	0.512991	7.08	Su et al., 2012
HT08-3	18	Spl lherzolite	3.17	49.4	0.704103	0.7041	0.40	2.08	0.512734	2.06	Su et al., 2012
HT08-4-1	18	lherzolite	3.22	27.9	0.704470	0.7044	0.23	1.13	0.512779	2.92	Su et al., 2012
HT08-5	18	Spl lherzolite	3.92	54.0	0.704076	0.7040	0.45	2.45	0.512964	6.56	Su et al., 2012
BG08-1	18	Spl lherzolite	9.10	139	0.704995	0.7049	0.61	3.14	0.512697	1.33	Su et al., 2012
BG08-2	18	Spl lherzolite	5.10	171	0.705578	0.7056	0.67	3.86	0.512787	3.12	Su et al., 2012
BG08-4	18	Spl lherzolite	6.68	202	0.704413	0.7044	2.54	14.7	0.512782	3.02	Su et al., 2012
HT7-1*	18	Harzburgite	4.13	45.3	0.704161	0.7041	0.37	1.92	0.512058	4.52	Unpublished data

-*Sr and Nd isotopic compositions of these samples were measured at the Center for Isotope Geochemistry, University of California at Berkeley. The $\varepsilon_{Nd}(t)$ values were calculated with reference to the $^{143}Nd/^{144}Nd$ of 0.511836 from the chondritic uniform reservoir (DePaolo, 1978).

- Whole-rock $^{87}Sr/^{86}Sr_i$ and $\varepsilon_{Nd}(t)$ values were calculated at 18 Ma.

Table DR8 **Trace element and Sr-Nd isotopic data for end-members used in geochemical modeling**

Geochemical end-members	Sr (ppm)	$^{87}Sr/^{86}Sr_i$	Nd (ppm)	$^{143}Nd/^{144}Nd_i$
Depleted mantle[1]	6.092	0.70217	0.483	0.51323
Primary kamafugite magma 1[2]	3526	0.70255	56.3	0.51309
Primary kamafugite magma 2[2]	3526	0.70410	56.3	0.51270
Carbonate-rich metasome in SCLM[3]	232	0.71052	2.79	0.51220
Phlogopite-rich metasome in SCLM[3]	100	0.73	5	0.51185
Carbonate-bearing pelagic sediment 1[4]	170	0.712	30	0.51200
Carbonate-bearing pelagic sediment 2[4]	110	0.722	60	0.51170

-[1] Trace element and Sr-Nd isotopic compositions of depleted mantle were from Workman and Hart (2005).

-[2] Because perovskite is an early-crystalizing phase, we thus calculated the Sr and Nd concentrations of primary kamafugite magma using average values of perovskite trace element data and partition coefficients between with katungite (D_{Sr} = 1.26, D_{Nd} = 51.1, Chakhmouradian et al., 2013). Sr-Nd isotopic compositions of primary melt 1 and 2 were set to be close to mantle sources with minor amounts of carbonate-bearing pelagic sediment.

-[3] Trace element and initial Sr-Nd isotopic compositions of carbonate-rich metasome in the SCLM beneath northeastern Tibet were based on the extrusive carbonatite at West Qinling (carbonatite sample 2013, Yu et al., 2004). Because of high Rb/Sr in phlogopite from mantle xenoliths, phlogopite-rich metasome were postulated to have extremely enriched Sr-Nd isotopic compositions due to radiogenic ingrowth.

-[4] Given that the contents of marine carbonate and prograde metamorphism have profound influence on the composition of subducting pelagic sediments (Ben Othman et al., 1989; Plank and Langmuir, 1998), different trace element concentrations and varying Sr-Nd isotopic compositions were used for modeling mantle metasomatism induced by sediment-derived melts. Because sediment 2 was postulated to have lower content of marine carbonate than sediment 1, it therefore had lower Sr, higher Nd, and more enriched initial Sr-Nd isotopic compositions.

- $^{87}Sr/^{86}Sr_i$ and $\varepsilon_{Nd}(t)$ values were calculated at 18 Ma.

References

Ben Othman, D., White, W.M., and Patchett, J., 1989, The geochemistry of marine sediments, island arc magma genesis, and crust-mantle recycling: Earth and Planetary Science Letters, v. 94, no. 1, p. 1–21, doi:10.1016/0012-821X(89)90079-4.

Chakhmouradian, A.R., Reguir, E.P., Kamenetsky, V.S., Sharygin, V.V., and Golovin, A.V., 2013, Trace-element partitioning in perovskite: implications for the geochemistry of kimberlites and other mantle-derived undersaturated rocks: Chemical Geology, v. 353, p. 112–131, doi:10.1016/j.chemgeo.2013.01.007.

Dai, L.-Q., Zhao, Z.-F., Zheng, Y.-F., An, Y.-J., and Zheng, F., 2017, Geochemical Distinction between Carbonate and Silicate Metasomatism in Generating the Mantle Sources of Alkali Basalts: Journal of Petrology, v. 58, no. 5, p. 863–884, doi: 10.1093/petrology/egx038.

Deng, W., 1989, Cenozoic volcanic rocks in the northern Ngari district of the Tibet (Xizang)-Discussion on the concurrent intracontinental subduction: Acta Petrologica Sinica, v. 5, no. 3, p. 1–11 (in Chinese with English abstract).

Deng, W., Zheng, X., and Yukio, M., 1996, Petrological characteristics and ages of Cenozoic volcanic rocks from the Hoh Xil Mts., Qinghai province: Acta Petrologica et Mineralogica, v. 15, no. 4, p. 289–298 (in Chinese with English abstract).

Dong, X., Zhao, Z., Mo, X., Yu, X., Zhang, H., Li, B., and DePaolo, D.J., 2008, Geochemistry of the Cenozoic kamafugites from west Qinling and its constraint for the nature of magma source region: Acta Petrologica Sinica, v. 24, no. 2, p. 238–248 (in Chinese with English abstract).

Dubois, J.C., Retali, G., and Cesario, J., 1992, Isotopic analysis of rare earth elements by total vaporization of samples in thermal ionization mass spectrometry: International Journal of Mass Spectrometry and Ion Processes, v. 120, no. 3, p. 163–177, doi: 10.1016/0168-1176(92)85046-3.

Ehrlich, S., Gavrieli, I., Dor, L.-B., and Halicz, L., 2001, Direct high-precision measurements of the 87Sr/86Sr isotope ratio in natural water, carbonates and related materials by multiple collector inductively coupled plasma mass spectrometry (MC-ICP-MS): Journal of Analytical Atomic Spectrometry, v. 16, no. 12, p. 1389–1392, doi: 10.1039/B107996B.

Goldstein, S.L., O'Nions, R.K., and Hamilton, P.J., 1984, A Sm-Nd isotopic study of atmospheric dusts and particulates from major river systems: Earth and Planetary Science Letters, v. 70, no. 2, p. 221–236, doi: 10.1016/0012-821X(84)90007-4.

Griffin, W.L., Powell, W.J., Pearson, N.J., and O'reilly, S.Y., 2008, GLITTER: data reduction software for laser ablation ICP-MS, *in* Sylvester, P., eds., Laser Ablation-ICP-MS in the earth sciences. Mineralogical association of Canada short course series, p 204–207.

Guo, P., Niu, Y., and Yu, X., 2014, A synthesis and new perspective on the petrogenesis of kamafugites from West Qinling, China, in a global context: Journal of Asian Earth Sciences, v. 79, p. 86–96, doi: 10.1016/j.jseaes.2013.09.012.

Isnard, H., Brennetot, R., Caussignac, C., Caussignac, N., and Chartier, F., 2005, Investigations for determination of Gd and Sm isotopic compositions in spent nuclear fuels samples by MC ICPMS: International Journal of Mass Spectrometry, v. 246, no. 1, p. 66–73, doi: 10.1016/j.ijms.2005.08.008.

Jacobsen, S.B., and Wasserburg, G.J., 1980, Sm-Nd isotopic evolution of chondrites: Earth and Planetary Science Letters, v. 50, no. 1, p. 139–155, doi: 10.1016/0012-821X(80)90125-9.

Jiang, D., Liu, J., and Ding, L., 2008, Geochemistry and petrogenesis of Cenozoic potassic volcanic rocks in the Hoh Xil area, northern Tibet plateau: Acta Petrologica Sinica, v. 24, no. 2, p. 279–290 (in Chinese with English abstract).

Jolivet, M., Brunel, M., Seward, D., Xu, Z., Yang, J., Malavieille, J., Roger, F., Leyreloup, A., Arnaud, N., and Wu, C., 2003, Neogene extension and volcanism in the Kunlun fault zone, northern Tibet: New constraints on the age of the Kunlun fault: Tectonics, v. 22, no. 5, p. 1052, doi: 10.1029/2002TC001428.

Kinny, P.D., Griffin, B.J., Heaman, L.M., Brakhfogel, F.F., and Spetsius, Z.V., 1997, SHRIMP U-Pb ages of perovskite from Yakutian kimberlites: Russian Geology and Geophysics, v. 38, p. 97-105.

Le Bas, M.J., 1989, Nephelinitic and basanitic rocks: Journal of Petrology, v. 30, no. 5, p. 1299–1312, doi: 10.1093/petrology/30.5.1299.

Le Maitre, R.W., 2002, Igneous Rocks: A Classification and Glossary of Terms: Cambridge, U.K., Cambridge University Press, p. 236.

Li, C., Fan, H., and Xu, F., 1989, Lithochemical characteristics of Cenozoic volcanic rocks in Qinghai-Xizang (Tibet) and its structural significance: Geoscience, v. 3, no. 1, p. 58–69 (in Chinese with English abstract).

Li, J., Bai, D., and Wang, X., 2004, Ages of volcanic rocks and planation surface in the Canmei Mountain area, northern Tibet: Geological Bulletin of China, v. 23, no. 7, p. 670–675 (in Chinese with English abstract).

Li, Q.-L., Li, X.-H., Liu, Y., Wu, F.-Y., Yang, J.-H., and Mitchell, R., 2010, Precise U–Pb and Th–Pb age determination of kimberlitic perovskites by secondary ion mass spectrometry: Chemical Geology, v. 269, no. 3, p. 396–405, doi: 10.1016/j.chemgeo.2009.10.014.

Liu, Y., Hu, Z., Gao, S., Günther, D., Xu, J., Gao, C., and Chen, H., 2008, In situ analysis of major and trace elements of anhydrous minerals by LA-ICP-MS without applying an internal standard: Chemical Geology, v. 257, no. 1–2, p. 34–43, doi: 10.1016/j.chemgeo.2008.08.004.

Ludwig, K.R., 2003, Isoplot/Ex Version 3.00: a Geochronological Toolkit for Microsoft Excel, *in*, eds., Berkeley Geochronology Center, Berkeley, CA, USA.

Lugmair, G.W., and Marti, K., 1978, Lunar initial $^{143}Nd/^{144}Nd$: Differential evolution of the lunar crust and mantle: Earth and Planetary Science Letters, v. 39, no. 3, p. 349–357, doi: 10.1016/0012-821X(78)90021-3.

Ma, Q., Zheng, J., Griffin, W., Zhang, M., Tang, H., Su, Y., and Ping, X., 2012, Triassic "adakitic" rocks in an extensional setting (North China): Melts from the cratonic lower crust: Lithos, v. 149, p. 159–173, doi: 10.1016/j.lithos.2012.04.017.

McFarlane, C.R.M., and McCulloch, M.T., 2007, Coupling of in-situ Sm–Nd systematics and U–Pb dating of monazite and allanite with applications to crustal evolution studies: Chemical Geology, v. 245, no. 1, p. 45–60, doi: 10.1016/j.chemgeo.2007.07.020.

Meng, F.-C., Yang, J.-S., Shi, R.-D., and Wu, C.-L., 2002, Origin of Miocene shoshonitic volcanic rocks from Xiongyingtai, Hoh Xil, North Xizang: Geochimica, v. 31, no. 3, p. 243–252 (in Chinese with English abstract).

Plank, T., and Langmuir, C.H., 1998, The chemical composition of subducting sediment and its consequences for the crust and mantle: Chemical Geology, v. 145, no. 3, p. 325–394, doi:10.1016/S0009-2541(97)00150-2.

Ramos, F.C., Wolff, J.A., and Tollstrup, D.L., 2004, Measuring $^{87}Sr/^{86}Sr$ variations in minerals and groundmass from basalts using LA-MC-ICPMS: Chemical Geology, v. 211, no. 1, p. 135–158, doi: 10.1016/j.chemgeo.2004.06.025.

Stacey, J.S., and Kramers, J.D., 1975, Approximation of terrestrial lead isotope evolution by a two-stage model: Earth and planetary science letters, v. 26, no. 2, p. 207–221, doi: 10.1016/0012-821X(75)90088-6.

Steiger, R.H., and Jäger, E., 1977, Subcommission on geochronology: Convention on the use of decay constants in geo- and cosmochronology: Earth and Planetary Science Letters, v. 36, no. 3, p. 359-362, doi: 10.1016/0012-821X(77)90060-7.

Stoppa, F., and Schiazza, M., 2013, An overview of monogenetic carbonatitic magmatism from Uganda, Italy, China and Spain: volcanologic and geochemical features: Journal of South American Earth Sciences, v. 41, p. 140–159, doi: 10.1016/j.jsames.2012.10.004.

Su, B.-X., Zhang, H.-F., Ying, J.-F., Tang, Y.-J., Hu, Y., and Santosh, M., 2012, Metasomatized lithospheric mantle beneath the western Qinling, Central China: insight into carbonatite melts in the mantle: The Journal of Geology, v. 120, no. 6, p. 671–681, doi: 10.1086/667956.

Sun, S.S., and McDonough, W.F., 1989, Chemical and isotopic systematics of oceanic basalts: implications for mantle composition and processes: Geological Society, London, Special Publications, v. 42, no. 1, p. 313–345, doi: 10.1144/GSL.SP.1989.042.01.19.

Turner, S., Arnaud, N., LIU, J., Rogers, N., Hawkesworth, C., Harris, N., Kelley, S., Van Calsteren, P., and Deng, W., 1996, Post-collision, shoshonitic volcanism on the Tibetan Plateau: Implications for convective thinning of the lithosphere and the source of ocean island basalts: Journal of Petrology, v. 37, no. 1, p. 45–71, doi: 10.1093/petrology/37.1.45.

Wang, J., and Li, J.P., 2003, Geochemical characteristics and geological implications of the Cenozoic kamafugites from Lixian County, West Qinling: Acta Petrologica et Mineralogica, v. 22, no. 1, p. 11–19 (in Chinese with English abstract).

Wasserburg, G.J., Jacobsen, S.B., DePaolo, D.J., McCulloch, M.T., and Wen, T., 1981, Precise determination of Sm/Nd ratios, Sm and Nd isotopic abundances in standard solutions: Geochimica et Cosmochimica Acta, v. 45, no. 12, p. 2311–2323, doi: 10.1016/0016-7037(81)90085-5.

Wei, Q., Li, D., Wang, G., and Zheng, J., 2007, Zircon SHRIMP U-Pb dating and geochemical characteristics of Chabaoma Formation volcanic rocks in northern Tibetan plateau and its petrogenesis: Acta Petrologica Sinica, v. 23, no. 11, p. 2727–2736 (in Chinese with English abstract).

Williams, I.S., 1998, U-Th-Pb Geochronology by Ion Microprobe, *in* McKibben, M.A., Shanks III, W.C., and Ridley, W.I., eds., Applications of microanalytical techniques to understanding mineralizing processes: Reviews in Economic Geology, Volume 7, Society of Economic Geologists, p. 1–35.

Workman, R.K., and Hart, S.R., 2005, Major and trace element composition of the depleted MORB mantle (DMM): Earth and Planetary Science Letters, v. 231, no. 1, p. 53–72, doi:10.1016/j.epsl.2004.12.005.

Wu, F.-Y., Yang, Y.-H., Mitchell, R.H., Li, Q.-L., Yang, J.-H., and Zhang, Y.-B., 2010, In situ U–Pb age determination and Nd isotopic analysis of perovskites from kimberlites in southern Africa and Somerset Island, Canada: Lithos, v. 115, no. 1, p. 205–222, doi: 10.1016/j.lithos.2009.12.010.

Wu, F.-Y., Arzamastsev, A.A., Mitchell, R.H., Li, Q.-L., Sun, J., Yang, Y.-H., and Wang, R.-C., 2013, Emplacement age and Sr-Nd isotopic compositions of the Afrikanda alkaline ultramafic complex, Kola Peninsula, Russia: Chemical Geology, v. 353, no. 5, p. 210–229, doi: 10.1016/j.chemgeo.2012.09.027.

Yang, J.-S., Wu, C.-L., Shi, R.-D., Li, H.-B., and Meng, F.-C., 2002, Miocene and Pleistocene shoshonitic volcanic rocks in the Jingyuhu area, north of the Qinghai-Tibet Plateau: Acta Petrologica Sinica, v. 18, no. 2, p. 161–176 (in Chinese with English abstract).

Yang, Y.-H., Wu, F.-Y., Wilde, S.A., Liu, X.-M., Zhang, Y.-B., Xie, L.-W., and Yang, J.-H., 2009, In situ perovskite Sr–Nd isotopic constraints on the petrogenesis of the Ordovician Mengyin kimberlites in the North China Craton: Chemical Geology, v. 264, no. 1, p. 24–42, doi: 10.1016/j.chemgeo.2009.02.011.

Yu, X., 1994, Cenozoic potassic alkaline ultrabasic volcanic rocks and its genesis in Lixian-Dangchang area, Gansu province: Sedimentary Geology and Tethyan Geology, v. 18, p. 114–129 (in Chinese with English abstract).

Yu, X., Mo, X., Flower, M., Su, S., and Zhao, X., 2001, Cenozoic kamafugite volcanism and tectonic meaning in west Qinling area, Gansu province: Acta Petrologica Sinica, v. 17, no. 3, p. 366–377 (in Chinese with English abstract).

Yu, X., Zhao, Z., Mo, X., Wang, Y.-L., Xiao, Z., and Zhu, D.-Q., 2004, Trace elements, REE and Sr, Nd, Pb isotopic geochemistry of Cenozoic kamafugite and carbonatite from west Qinling, Gansu Province: Implication of plume-lithosphere interaction: Acta Petrologica Sinica, v. 20, no. 3, p. 483–494 (in Chinese with English abstract).

Yu, X., Zhao, Z., Zhou, S., Mo, X., Zhu, D.-Q., and Wang, Y.-L., 2006, $^{40}Ar/^{39}Ar$ dating for Cenozoic kamafugite from western Qinling in Gansu Province: Chinese Science Bulletin, v. 51, no. 13, p. 1621–1627, doi: 10.1007/s11434-006-2010-7.

Yu, X., Mo, X., Zhao, Z., Huang, X., Li, Y., Chen, Y., and Wei, Y., 2009, Two types of Cenozoic potassic volcanic rocks in West Qinling, Gansu Province: Their petrology, geochemistry and petrogenesis: Earth Science Frontiers, v. 16, no. 2, p. 79–89 (in Chinese with English abstract).

Yu, X., Mo, X., Zhao, Z., He, W., and Li, Y., 2011, Cenozoic bimodal volcanic rocks of the West Qinling: Implication for the genesis and nature of the rifting of north-south tectonic belt: Acta Petrologica Sinica, v. 27, no. 7, p. 2195–2202 (in Chinese with English abstract).

Zhao, Z.-M., Ji, W.-H., Li, R.-S., Ma, H.-D., Yang, Z.-J., Wang, B.-Z., Zhu, Y.-T., Wang, G.-C., Bai, D.-Y., Zhang, Z.-F., and Li, D.-P., 2009, Geochemical characteristics and petrogenesis of volcanic rocks since the Neogene in the Bayankala and east Kunlun region, northern Tibetan plateau: Geochimica, v. 38, no. 3, p. 205–230 (in Chinese with English abstract).

Zheng, X., and Bian, Q., 1996, On the Cenozoic volcanic rocks in Hoh Xil District, Qinghai Province: Acta Petrologica Sinica, v. 12, no. 4, p. 530–545 (in Chinese with English abstract).

Zhu, Y.-T., Jia, Q.-X., Yi, H.-S., Lin, J.-H., Shi, L.-C., Peng, C., and Guo, T.-Z., 2005, Two periods of Cenozoic volcanic rocks from Hoh Xil lake area, Qinghai: Journal of Mineralogy and Petrology, v. 25, no. 4, p. 23–29 (in Chinese with English abstract).

Zindler, A., and Hart, S., 1986, Chemical geodynamics: Annual Review of Earth and Planetary Sciences, v. 14, p. 493–571, doi:10.1146/annurev.ea.14.050186.002425.